Thermal Annealing and Superconductivity
in
Zr Based Metallic Glasses

Thesis by
Gillian E. Marshall

In partial fulfillment of
the requirements for the
Degree of Master of Science

Department of Physics
McGill University
Montreal, Quebec

1986

(submitted May 28, 1986)

for
David V. Baxter

It was the best of times,
it was the worst of times,
it was the age of wisdom,
it was the age of foolishness
- Charles Dickens

Abstract

The effects of annealing of the superconducting transition temperature of zirconium-based metallic glasses were studied. Mostly binary glasses were examined; the second element was one of Cu, Ni, Co, or Fe. Both irreversible and reversible structural relaxation processes were examined.

For Fe-Zr in the range 75-80 at% Zr T_c demonstrates an initial irreversible increase upon annealing at 488 K. Inclusion of spin-fluctuations into the McMillan equation account for both the behaviour of Fe-Zr and trends in T_c with changes in composition.

Studies on the reversible component show that very small reversible changes in T_c may be effected in Cu-Zr and Ni-Zr, none in either Fe-Zr or Co-Zr. This contrast may be understood in terms of different rates of atomic diffusion.

Résumé

On a etudié les effets de recuits à basses températures sur la température critique de métaux amorphes supraconducteurs contenant du zirconium. La plupart des alliages étudiés étaient binaires et le deuxième élément était parmi les suivants: Cu, Ni, Co, ou Fe. On a observé des changements réversibles et irréversibles.

Pour Fe-Zr avec 75-80 at% Zr, il y a une augmentation de T_c irréversible quand l'échantillon est recuit a 488 K pour de courtes périodes de temps. L'inclusion de fluctuations de spin dans l'équation de McMillan explique bien comment se comporte Fe-Zr, et explique aussi les changements de T_c pour les autres alliages.

Des petits changements réversibles de T_c ont été remarqués dans Cu-Zr et Ni-Zr, mais n'ont pas été remarqués dans Fe-Zr ou Co-Zr. Ces différences peuvent être attribuées aux différentes vitesses de diffusion des atomes dans ces quatres types de métaux amorphes.

Acknowledgements

I would like to acknowledge the support of both Professor John Strom-Olsen and Dr. Zaven Altounian, for providing the opportunity to perform this research and for introducing me to the field of metallic glasses.

I would also like to express my thanks for the technical support of Frank VanGills. In preparing the manuscript, help with the IBM word processor from Hazel Carinci, Professor Mark Sutton and Ian Graham was greatly appreciated. I could not possibly overstate how much the friendship and discussions with various members of the fourth floor has meant to me, especially Dr. David Baxter, Ian Graham, Reinhart Richter, and Stefan Idziak.

I would especially like to thank my family for constant encouragement. My heartfelt thanks go out to Seidokwan, my judo club, for throwing me around and, from time to time, allowing me to throw them around. In particular I thank my sensei, Don Niiya, for instilling me with some measure of selfconfidence.

Financial support was received from McGill University in the form of teaching assistantships and a Carl Reinhardt bursary, from the Natural Sciences and Engineering Research Council of Canada (NSERC), and from Fonds pour la Formation de Chercheurs et l'Aide a la Recherche (FCAR). The financial support was greatly appreciated.

Table of Contents

Table of Contents (cont.)

List of Figures

List of Figures (cont.)

List of Figures (cont.)

List of Tables

Chapter 1 - Introduction

Amorphous solids are solids lacking long range atomic periodicity. They have been known to mankind for centuries, ordinary window glass being a common example. Amorphous metals also lack long range atomic periodicity, but, as a distinction from the broader class of amorphous materials, also possess normal metallic properties. These have recently been developed using a variety of techniques including vapour deposition, electrodeposition, and sputtering. Amorphous metals were first produced using the technique of vapour deposition as early as 1934(1.1). This was very interesting from the point of view of physics, but was not practical due to the very small amount of material produced. This problem was not overcome until the advent in 1960 of methods for rapidly quenching metals into the amorphous state from the liquid(1.2). The most popular technique of rapid quenching is the so-called "melt-spinning" technique which permits the production of amorphous metals in industrial quantities. Melt-spinning is the technique used to produce the metallic glasses for this work, and is described in Chapter 2.

Metallic glasses are a subgroup of the broad class of amorphous metals. The term "metallic glass" is now generally reserved for amorphous metals quenched from the melt. They have recently received much attention because of their interesting properties characteristic of an amorphous material, coupled with the possibility of production of large quantities.

To produce a metallic glass an ingot of the desired constituent composition is heated above the liquid temperature and then cooled very quickly. A very high cooling rate is required in order to undercool the liquid below the so-called glass temperature T_g, (defined typically by the viscosity $\eta \geq 10^{13}$ poise) before significant nucleation of the crystal phase occurs. The glass is then a configurationally frozen liquid, a metastable state at room temperature for many alloys. The time-temperature-transformation (T-T-T) diagram in figure 1.1 shows schematically how long a glass at a given temperature will take to crystallize. The diagram illustrates the time required for a certain fraction of the sample (typically 1 in 10^6) to transform. The crystal phase makes a "nose" under which there is glass. The nose, at approximately the glass temperature T_g, indicates that the liquid does not crystallize readily at high temperatures because of thermal vibrations, nor at low temperatures because of the high viscosity induced by low temperatures. The tip of the nose indicates the optimal temperature for crystallization. In order to avoid crystallization in the glass forming process it is necessary to cool the alloy from the liquid temperature fast enough to avoid the nose of crystallization. The minimum cooling rate is thus determined, as shown in figure 1.1.

It has been observed that metallic glasses form near deep eutectics of the constituent elements. This can be explained as follows: although the glass temperature T_g is approximately constant for the glass systems

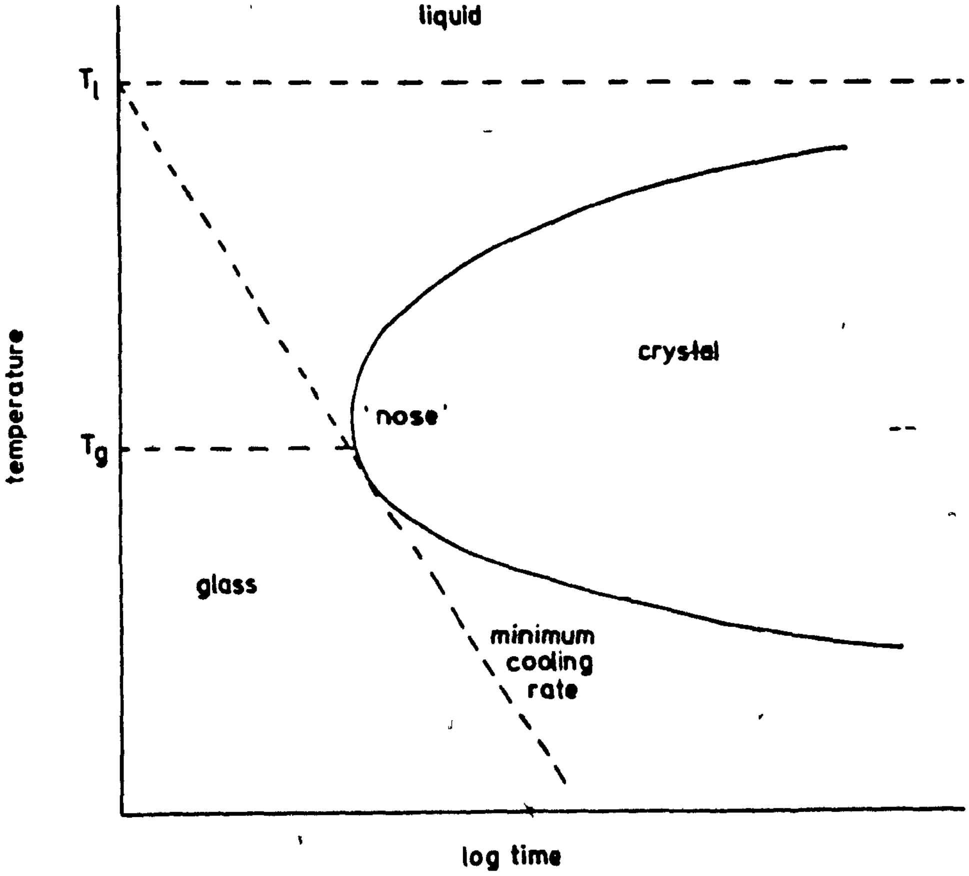

figure 1.1 Schematic time-temperature-transformation (T-T-T) diagram showing the 'nose' of crystallization and the minimum cooling rate required to avoid crystallization of a sample

used, the equilibrium melting temperature T_l varies dramatically. We know that in certain alloys (those where the components have a large negative heat of mixing) the equilibrium melt temperature is substantially lower than for the pure constituents. This leads to one or more sharp minima, called eutectics. Since the cooling rate depends on the difference T_l-T_g, glasses are easier to make for a small cooling rate, hence for small T_l, which is found at deep eutectics. This observation that metallic glasses form near deep eutectics of the constituent elements has been useful in making new glasses.

It is convenient to divide metallic glasses into two distinct categories. The first is one whose constituent elements comprise a transition metal or noble metal and a metalloid of group III, IV, or V. The metalloid acts as a glass former or stabilizer. The second empirical category is one whose constituent elements are only metallic. Examples of the former are Fe-B, Fe-Ni-P-B, and Pd-Si, while examples of the latter are Fe-Zr, Co-Zr, and Y-Al. The present work involves only metallic glasses from the second category, specifically Fe-Zr, Co-Zr, Ni-Zr, Cu-Zr, and Cu-Ni-Zr.

When a metallic glass is formed it is not necessarily at a local minimum of free energy. This is shown by the fact that its characteristics change when it is annealed. The changes fall into two distinct categories: reversible and irreversible. The present work examines both types of process.

When a sample is annealed the predominant change in characteristics is irreversible. The irreversible change can be divided into two processes: nucleation, which results in the eventual crystallization of the sample, and what is believed to be changes in the topological short range order (TSRO). TSRO can be understood using the idea of free volume. As quenched metallic glasses have quenched in voids so that they have a specific volume that is larger, perhaps by as much as 1%, than the specific volume of the same glass when fully relaxed. This excess specific volume is termed "free volume", and plays an important role in physical properties. Annealing an as quenched metallic glass at temperatures well below the crystallization temperature T_x partly anneals out the free volume. In changing the free volume the characteristics of the glass are then changed.

It has been demonstrated in some glasses(1.3)(1.4), however, that it is possible to move reversibly between metastable states created at different temperatures of annealing. Some authors, notably Egami(1.5), suggest that this reversible process is the result of changes in chemical short range order (CSRO). CSRO is most easily understood using the idea of a state of mixture of the alloy. When quenched, a completely random mixture of the alloy is not attained, so the chemical composition about each atom is different from the average. This gives the alloy chemical short range order. Egami in particular has suggested that the local configuration, or CSRO of the atoms can be changed reversibly by annealing the alloy at different temperatures. This could be the cause of the reversible component of relaxation observed in some metallic glasses. If this hypothesis is correct then we should expect to see a larger effect in a ternary glass where two of the constituent elements are very similar than in a binary glass where only one of the two similar elements is present. In the ternary glass one would expect a larger rearranging of the two similar elements. The systems Cu-Zr, Ni-Zr, and (CuNi)-Zr were chosen to compare and thus to examine in this way the validity of Egami's model. It should be noted that most of the data supporting Egami's model is from ternary boron-based glasses.

Properties used to study this reversible relaxation effect include Curie temperature(1.3) and magnetic anisotropy(1.6). In the present work we have examined the influence of thermal annealing on the superconducting transition temperature T_c. T_c for the systems chosen occurs in the convenient range of 1 to 4 K, can be measured precisely, and varies significantly upon annealing. For these reasons T_c was chosen as a monitor of the relaxation behaviour of the chosen systems.

Anderson et al.(1.4) examine the effect of annealing a $Ni_{24}Zr_{76}$ glass isochronally for short periods of time at temperatures below 300°C. They find that at these temperatures the relaxation process, seen through the superconducting transition temperature T_c appears to have a reversible component. The present work extends the work of reference 1.4 by examining the behaviour of Ni-Zr, Cu-Zr, Ni-Cu-Zr, Co-Zr, and Fe-Zr, and by making a comparison of the relaxation behaviour of the different alloys.

Because of the changes in glasses upon annealing, a thorough understanding of the effects of low-temperature annealing of metallic glasses is important for an adequate a priori prediction of the macroscopic properties of the glasses. It is the purpose of the present work to extend the understanding of the effects on the superconducting transition temperature T_c of annealing metallic glasses at temperatures well below T_x.

There are two common methods of measuring T_c. The easiest method is to measure electrical resistance using the property that superconducting materials have zero dc electrical resistivity. The present work, however, uses the Meissner effect, that superconductors in weak magnetic fields are perfectly diamagnetic, having zero magnetic induction in their interior. Thus when a sample is placed in a magnetic field and cooled through its superconducting transition temperature, the magnetic flux originally present is ejected from the sample, as shown in figure 1.2.

Measuring T_c through resistance is generally much easier to do and is therefore a more common method. However measuring T_c with a susceptibility bridge as in the present work has the advantage that it is a bulk measurement. Should the sample be very inhomogeneous so that there are, for example, two regions with two different transition temperatures, only the higher temperature will be measured by the resistance method and

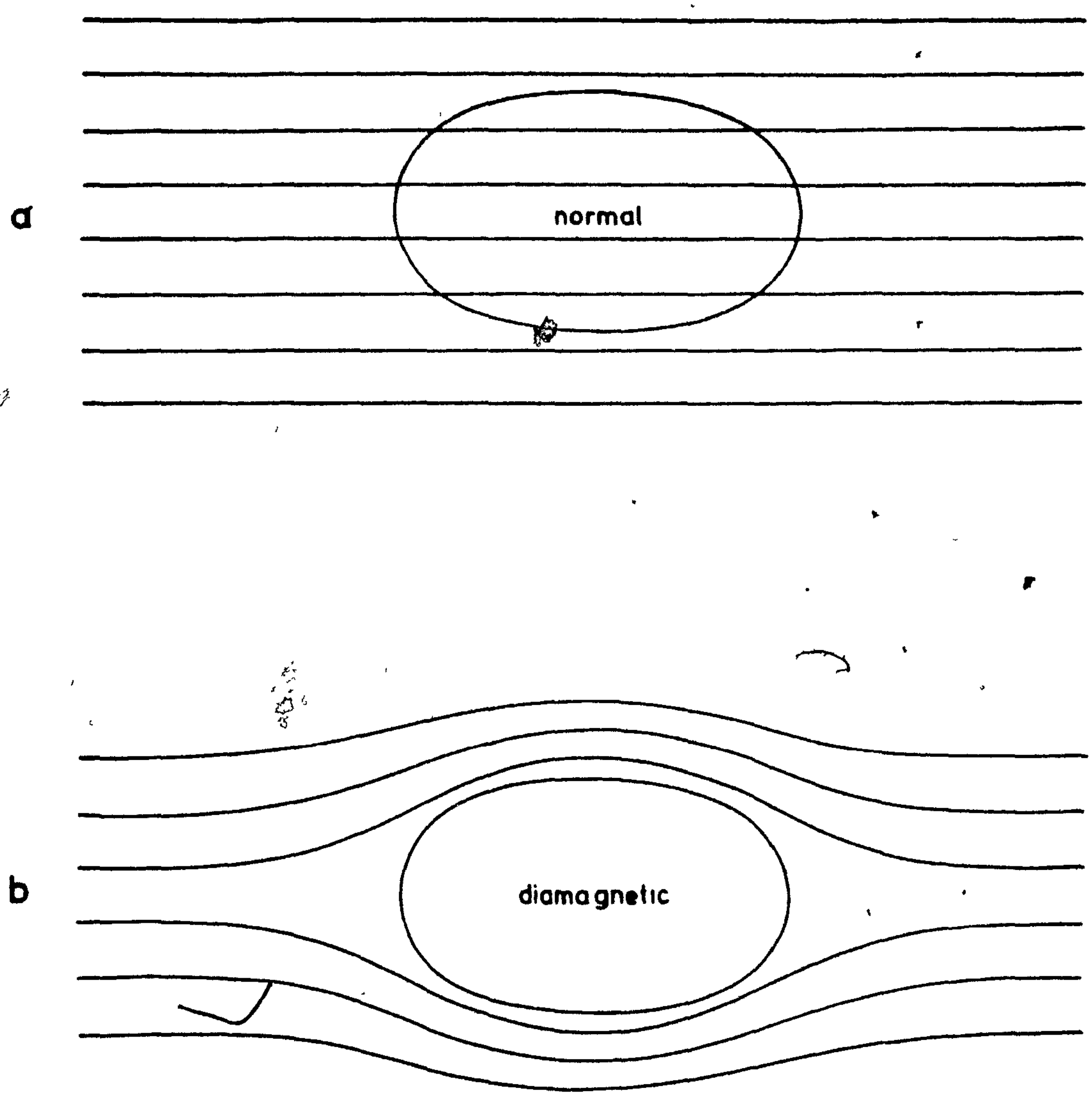

figure 1.2 Schematic diagram of Meissner effect

a) a normal metal in a weak magnetic field

b) a superconductor in a weak magnetic field, exhibiting the property of perfect diamagnetism the inhomogeneity will go undetected. By using the Meissner effect, if there are two transition temperatures there should be two distinct jumps in the mutual inductance. It has been suggested(1.7) that the Ni-Zr system can show such an inhomogeneity.

It should be noted that superconductors fall into two categories: type I and type II superconductors. Amorphous superconductors fall in the latter category which is the "dirty limit" of the theory. From the theory of Abrikosov and Gorkov(1.8) the type of a superconductor is determined by the Ginzburg-Landau parameter κ:

$$\kappa = \frac{\lambda(T)}{\xi(T)} = \frac{\text{penetration depth}}{\text{coherence length}} \qquad (1.1)$$

Type II superconductors have $\kappa > \frac{1}{\sqrt{2}}$. Amorphous superconductors are typically(1.9) in the range of $\kappa \sim 40\text{-}100$, so are classed extremely dirty superconductors. The fundamental difference between type I and type II superconductors is that type I superconductors are homogeneous, while type II superconductors exist in a mixed state, part normal and part superconducting. Type II superconductors transform at the lower critical field, H_{c1}, from a homogeneous superconducting state to a mixed state; the upper critical field, H_{c2}, is the highest field at which the mixed state can exist.

The following is a brief description of the major interactions causing superconductivity, with a small development leading to the commonly used McMillan equation describing T_c. Although a full understanding of the nature of the superconducting state for real materials has not yet been achieved, the nature of the two basic interactions responsible is known. They are the electron-phonon and the screened Coulomb interactions.

First, consider the electron-phonon interaction. A displacement of one ion in a lattice of positive ions of a metal causes a change in the crystal field and so produces a force on neighbouring ions. The ions are thus coupled, forming a system of coupled oscillators whose excitations are called lattice waves or phonons. The electron-phonon interaction arises from the fact that when an electron moves through the lattice, nearby ions are drawn towards it. This creates an excess in positive charge where the electron had been and a second electron is drawn towards this excess positive charge. This is the basis of the phonon mediated electron interaction, or the electron-phonon interaction.

Now consider the Coulomb interaction. The electrons in a metal can be considered as being a free gas of electrons. Due to the charge at one point other charges in the metal are rearranged and this offsets the Coulomb potential. This leads to an effective two body screened interaction of the form(1.10)

$$V(r) = \frac{Ze^2}{r} e^{-\lambda r} \qquad (1.2)$$

where r is the distance away from the point charge Z. This indicates that the inter-electron potential is of the coulombic form times an exponential damping factor and the damping factor has the effect of reducing the potential to negligible size at distances greater than ~ $1/\lambda$. λ is typically of the order of k_F for metals so there is an effective screening at distances greater that the interparticle spacing. Thus the Coulomb repulsion between two electrons is reduced in metals, both in strength and in range, by the collective screening effect of other electrons. This reduced Coulomb repulsion is the so-called screened Coulomb effect which plays a role in superconductivity.

The sum of the electron-phonon and screened Coulomb interactions results in an apparent small net attraction between pairs of electrons. As was first shown by Bardeen, Cooper, and Schrieffer(1.11), such an interaction can lead to a collective bound state of 'Cooper pairs' of electrons. From the resulting Hamiltonian the BCS theory deduces a simple relationship between critical temperature T_c and electron-phonon interaction to predict T_c:

$$T_c = 1.14\langle\omega\rangle\exp\left(-\frac{1}{N(0)V}\right) \tag{1.3}$$

where $\langle\omega\rangle$ is a typical phonon energy and $N(0)V$ the electron-phonon interaction strength which arises from $N(0)$, the electron density of states at the Fermi surface and V, the electron pairing potential. The major limitations of this theory are that the the Coulomb interaction is ignored, and the interaction between electrons and phonons is assumed small, while it is known that this second condition is not fulfilled for all superconductors.

Later, the theory was developed further(1.12) to include the retarded nature of the electron-phonon interaction which did not have to be assumed small, and the retarded Coulomb interaction. The drawback of these theories was that they required numerical solutions.

McMillan(1.13) developed the existing theory for so-called "weak coupling" to arrive at the form of the eventual T_c equation. Experimental data was then taken to find appropriate values for certain numerical coefficients. The McMillan equation was thus

$$T_c = \frac{\Theta_D}{1.45} \exp\left(- \frac{1.04(1+\lambda_{ep})}{\lambda_{ep} - \mu^*(1 + 0.62\lambda_{ep})}\right) \tag{1.4}$$

where the Debye temperature Θ_D is taken for the characteristic phonon frequency, λ_{ep} is the electron-phonon coupling constant, and μ^* the retarded Coulomb potential parameter. Note that the numerical coefficients are simply the result of numerical integration. Since the equation is approximate it is usually adequate to replace it by:

$$T_c = \frac{\Theta_D}{1.45} \exp\left(- \frac{1+\lambda_{ep}}{\lambda_{ep}-\mu^*}\right) \tag{1.5}$$

This equation for T_c is now the basis for comparison for most experimental results. Further developments to account for spin-fluctuations are discussed in Chapter 4.

To summarize, the present work examines the effects of annealing metallic glasses. The macroscopic property used to monitor changes in the sample is the superconducting transition temperature T_c, and is measured using the Meissner effect. The samples used are type II superconductors, and the theory used to analyze the data is based on the McMillan equation since the samples used are in the weak coupling limit. Systems are examined and compared where spin-fluctuations are negligible and the system Fe-Zr, where spin-fluctuations are significant, is analyzed. As well as the above irreversible effects a reversible component is examined in many of the systems. These topics are examined here because a thorough understanding of the interactions affected by annealing is necessary for a complete understanding of the macroscopic characteristics of the glasses.

The ensuing chapters are organized as follows. Chapter 2 contains an explanation of the experimental methods used. Results are presented in Chapter 3 and are then discussed fully in Chapter 4. Finally the most important conclusions are summarized in Chapter 5.

Chapter 2 - Experimental Procedures

2.1 Sample Preparation

Samples were prepared by arc-melting the appropriate elements to form small ingots which were then rapidly quenched. The pure elements used were obtained from Alfa products, Massachussets, the purities, morphology, and etchant for which are listed in table 2.1.

Table 2.1

A list of the purity and the morphology of the elements used and their corresponding etchants

element	purity(%)	morphology	etchant
cobalt	99.998	5mm diameter rod	HCl/H_2O_2 (3:2)
copper	99.999+	9.5mm diameter rod	H_2O/HNO_3 (3:1)
iron	99.98	random lump	-------
nickel	99.998	5mm diameter rod	HF/HNO_3 (1:1)
zirconium	99.95	crystal bar	$H_2O/HF/H_2O_2$ (20:1:1)

Appropriate amounts of the pure elements were weighed and then etched to within 0.005% of the desired compositions. Etching was performed in order to obtain the precise composition and to remove impurities left by the cutting tools. The elements were etched and then quickly immersed in distilled water to stop any further reaction. The iron lump showed no signs of oxidation, and was not etched due to the high risk of oxidation immediately after being removed from the etchant.

To form ingots, the appropriate constituents were arc-melted under a titanium-gettered argon atmosphere. The nominal compositions of the binary and ternary samples made are $Co_{25}Zr_{75}$, $Ni_{25}Zr_{75}$, $Cu_{25}Zr_{75}$, $Ni_{33}Zr_{67}$, $(CuNi)_{33}Zr_{67}$, $Fe_{25}Zr_{75}$, and $Fe_{20}Zr_{80}$. Ingots, typically of 1-2 g were remelted several times, then turned over and remelted several more times to ensure homogeneity. Ingots displaying much oxidation at this point were discarded. The amount of oxidation was determined qualitatively by the colour of the ingot. Good ingots displayed a clean, shiny surface while ingots displaying a yellow tint to the surface were discarded. The ingots were then weighed a second time; in all cases the mass was found to differ from the original mass of the constituent elements by less than 0.1%. Once rapidly quenched the composition of the samples was verified against published results for superconducting and crystallization temperatures, and using a scanning electron beam microprobe. The results indicate that the nominal compositions were correct to within 1%, as will be discussed in Chapter 3. In all cases samples are refered to by their nominal composition.

Ribbons were then spun from the ingots using the melt-spinning apparatus shown in figure 2.1. The ingot was placed in a quartz crucible and heated by an induction coil powered by a LEPEL High Frequency RF

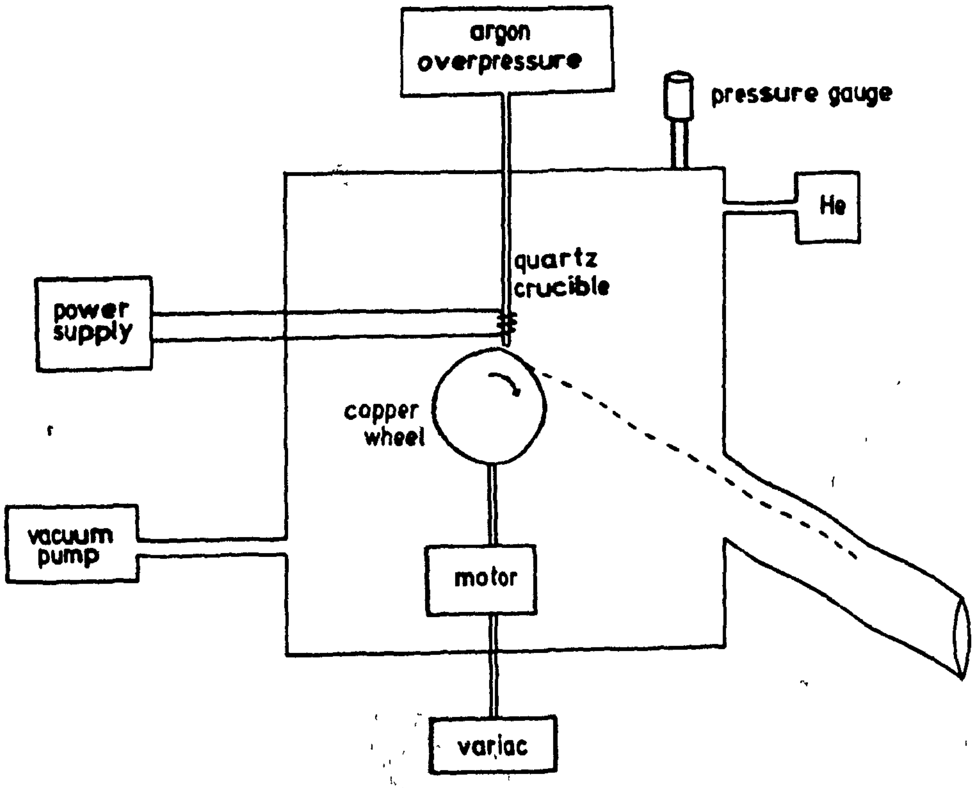

figure 2.1 Melt-spinning equipment

generator. The molten ingot was then ejected from the crucible through an orifice, typically of diameter 0.5-1.0 mm, by an overpressure of approximately 25 KPa (7 in of Hg) of high-purity ($0_2 \leq 3$ ppm) argon gas, on to a highly polished copper wheel, rotating at a tangential velocity of about 50 m/s.

Parameters having an effect on the quality of the glass are the cooling rate c and the tangential velocity v of the copper wheel. Also the position of the sample within the induction coil and the power P used to heat the ingot affect the temperature to which the ingot is heated before ejection from the crucible. Each sample was spun using the same parameters to validate comparison between them on the basis of composition alone. The tangential velocity v was held at approximately 50 m/s. The voltage to the induction coil was held at 40-45 V, though the inability to place the sample in exactly the same place led to variations in heating rates. The cooling rate can be calculated as follows. The liquid can be considered striking the surface of the wheel at a temperature T_m, then remaining in contact with the wheel over a distance d, where the wheel rotates at a constant tangential velocity v, and then leaving the wheel at a temperature well below the glass transition temperature. The appropriate equation is

$$c = \frac{\Delta T}{d/v} \qquad \text{...} \qquad (2.1)$$

The distance d has been estimated in the laboratory from similar quenches using high speed photography. Typically d is about 2 cm. The melt temperature of the alloys is about 1200 K and their glass temperature about 500 K. This gives a quench rate of order 1.8×10^6 K/s for a tangential velocity of 50 m/s. Ribbons produced were 1-3 m long, 1-2 mm wide and 20-30 μm thick. All ribbons were extremely ductile at this stage and none showed any sign of oxidation in the form of suface discolouration.

2.2 Differential Scanning Calorimetry (DSC) and X-ray Diffraction

Once spun, all ribbons were subjected to Differential Scanning Calorimetry (DSC) to check the crystallization characteristics. The instrument used is a Perkin-Elmer DSC-2C. A DSC measures the rate at which energy is either emitted or absorbed by a sample, as compared to an empty reference pan. Both the sample and reference have their respective heaters set to control the desired temperature or heating rate. Such measurements are useful because any changes in structure such as nucleation or crystallization are related to a change in enthalpy of the system, which can be measured by a DSC . From analysis of the data we can determine the activation energy E_a, the crystallization temperature T_x, and the change in enthalpy δH of crystallization. Measuring the change in enthalpy can be done either as a function of temperature for a constant rate of increase of temperature (isochronal) or as a function of time for a constant temperature (isothermal). In the present work all DSC measurements to determine the quality of the glasses were isochronal and T_x and E_a were determined.

For DSC measurements samples of roughly 10 mg were placed in an aluminum pan of roughly 15 mg and covered with an aluminum cover. The aluminum pan was placed in a platinum sample holder. An identical empty aluminum pan and cover were placed in a reference platinum sample holder. Each sample holder has its own carefully balanced heating coil and thermometer. The circuit used is shown in figure 2.2. Results of the DSC measurements for the as quenched glasses showed good agreement with previously obtained results for metallic glasses of the nominal compositions(2.1).

The present project required the samples to undergo extensive annealing. After annealing it was desirable to detect the specific phases that crystallized or to check whether crystallization had occured. For this a NICOLET L2 automated powder diffractometer was used. The diffractometer was capable of resolving 1-2% crystallization. Incoming CuK_α X-rays of 1.542 A wavelength were diffracted by the flat samples. The scattered X-ray beam was passed through a monochrometer and detected by a NaI(Ti) scintillation detector, as shown in figure 2.3. The geometry of the diffractometer is that of the standard Bragg-Brentano X-ray powder diffractometer(2.2). For this particular diffractometer the sample is

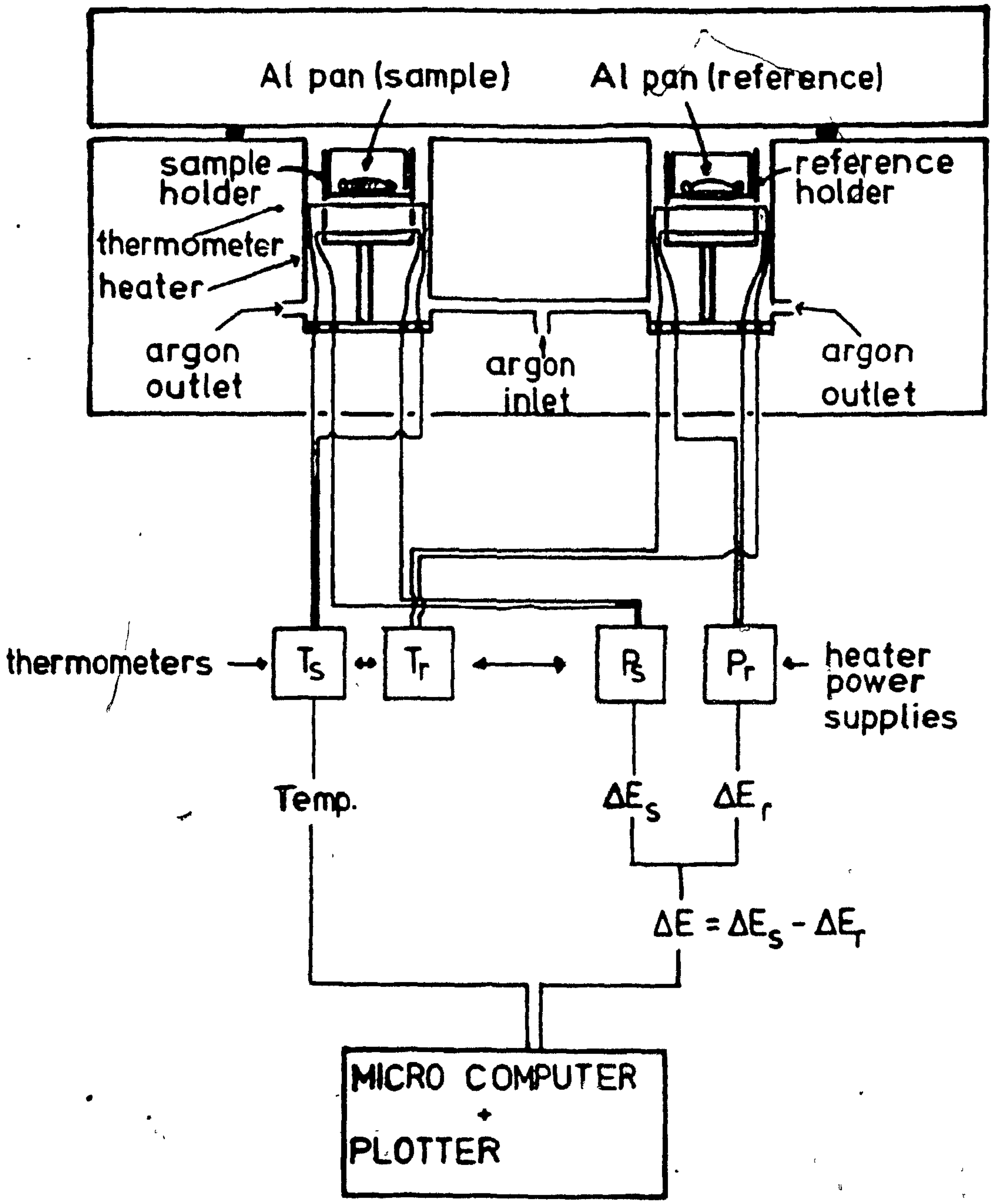

figure 2.2 Differential Scanning Calorimeter (taken directly from reference 2.3)

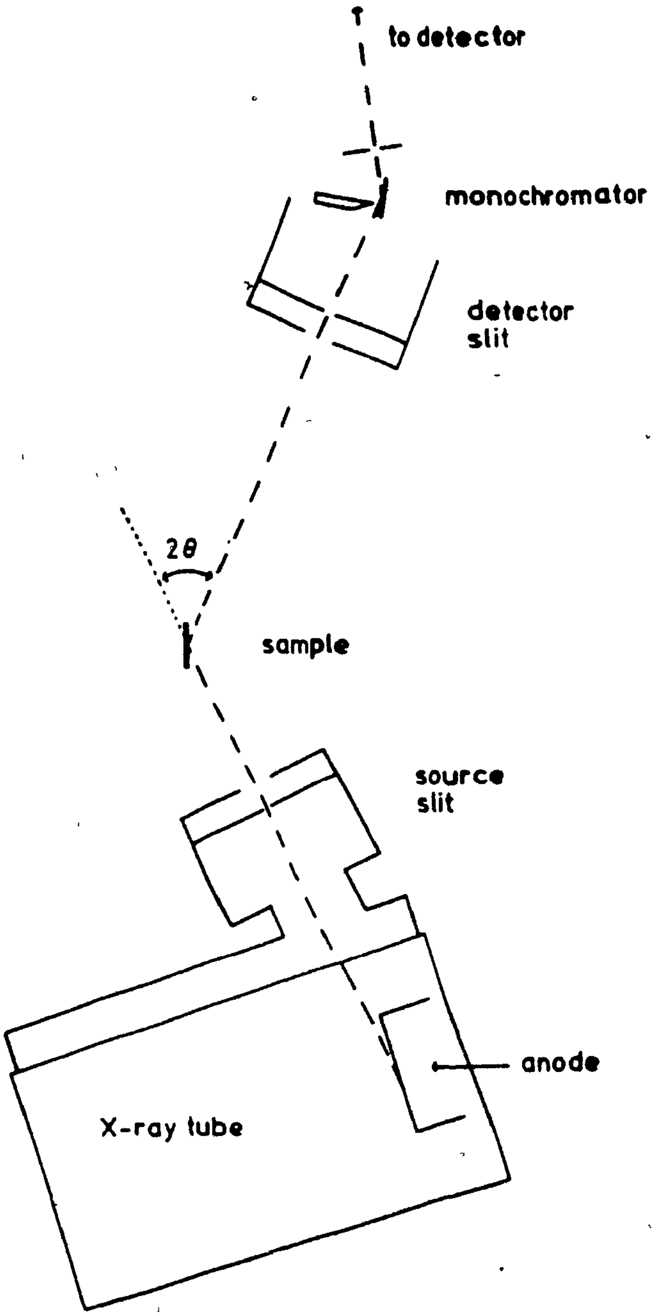

figure 2.3 X-Ray Powder Diffractometer showing the reflection geometry

mounted on a flat piece of glass and is held in place by some double stick tape.

2.3 Annealing Techniques

The samples were annealed at different temperatures and for different periods of time. Anneals for periods of time not exceeding three hours were performed in the DSC using the isothermal mode. When only one measurement was required of a sample it was made two cm long, since this had been chosen as the standard sample length for measurement of the superconducting transition temperature (see below). Where many samples were required to undergo identical short anneals it was more convenient to anneal them together in the DSC using many pieces of 3-5 mm length. To anneal the samples either one piece of two cm or many pieces of 3-5 mm were placed in an aluminum pan and covered with an aluminum cover. Samples of two cm were wrapped around the inside of the aluminum pan while the smaller samples were placed in the bottom of the pan. The samples were brought up to temperature at a rate of 320°C/min, were annealed at the given temperature for the specified time and then cooled down to room temperature again at the same rate.

Longer anneals were performed in a horizontal furnace built in the laboratory (see figure 2.4). The sample, in a pyrex tube evacuated to 5×10^{-6} Torr, was centered with respect to the furnace. The temperature

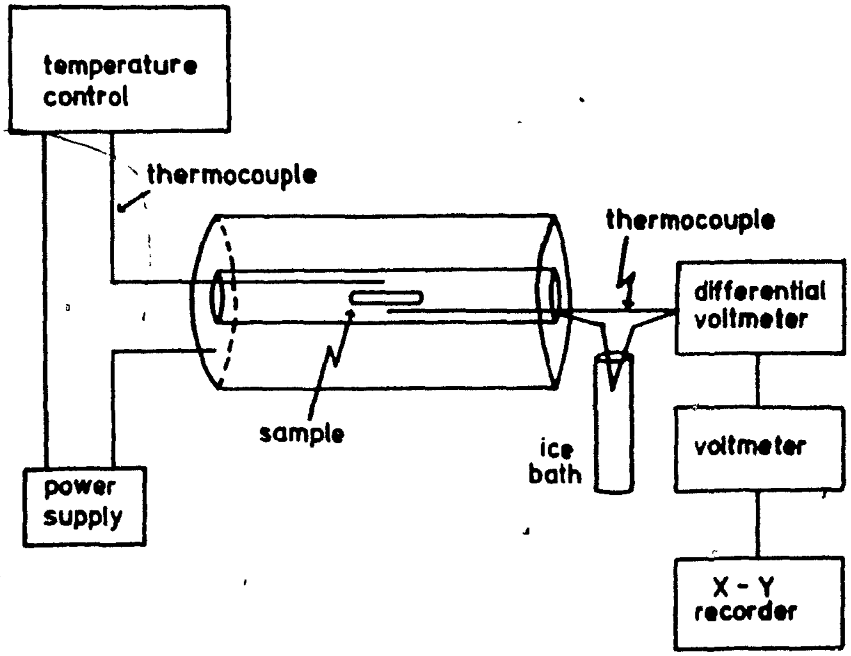

figure 2.4 Horizontal furnace used for annealing samples for times exceeding three hours

was set using a Honeywell Pyr-O Vane analog meter, and was monitored by a standard thermocouple centered with respect to the furnace. In this arrangement it was found that the average sample temperature was 10-15°C colder than the pre-set value. So the sample temperature was measured by a chromel-alumel thermocouple whose reference junction was placed in an ice bath. Fluctuations about the mean of the temperature of the furnace depended on the power setting. If the power setting was too high the furnace continued to heat up after reaching its upper allowable temperature; if the power setting was too low the furnace took too long to reach optimal temperature. Both cases contributed to large error in the temperature. By adjusting the power setting it was found possible to stabilize the furnace temperature to within ± 3°C.

2.4 Superconducting Transition Temperature (T_c) Measurements

The superconducting transition temperature T_c was measured through the Meissner effect using an ac susceptibility bridge as mentioned in Chapter 1. In this bridge there was a primary coil surrounding two secondary coils (see figure 2.5). The two secondaries were wound as an astatic pair so that the mutual inductance between the primary and secondaries was zero in the absence of any sample. The sample was placed inside one of the secondaries and held in place at one end with a dab of Dow Corning high vacuum grease to ensure consistent positioning of the sample (see figure 2.6). An ac current was put through the primary which induced a magnetic field in both of the secondary coils. The induction in the secondary coil containing the sample differed from the empty secondary by the amount of the sample magnetization. The difference in induced voltages $V_A - V_B$ was then observed as a function of temperature. When the sample became superconducting the magnetic flux originally present was ejected from the sample. This made a change in $V_A - V_B$ which was readily measurable.

The magnetic field induced by the current in the primary is:

$$H = N I$$

and the magnetic induction is:

$$\begin{aligned} B &= \mu_0 H \\ &= \mu_0 N I \end{aligned}$$

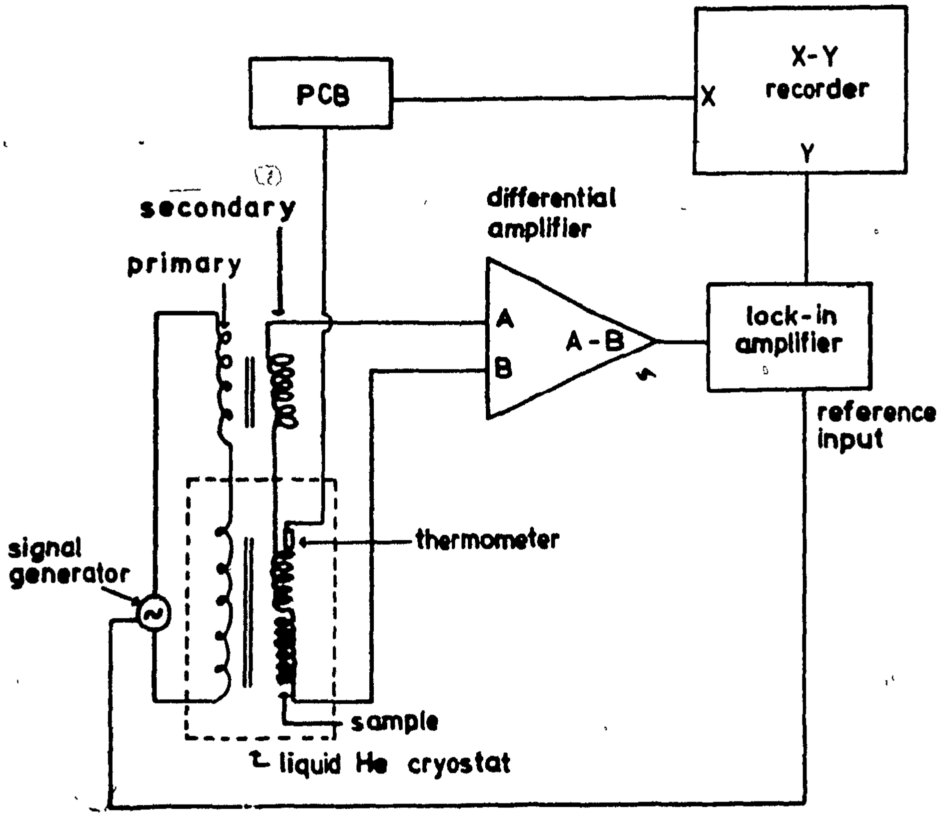

figure 2.5 Circuit for ac susceptibility bridge

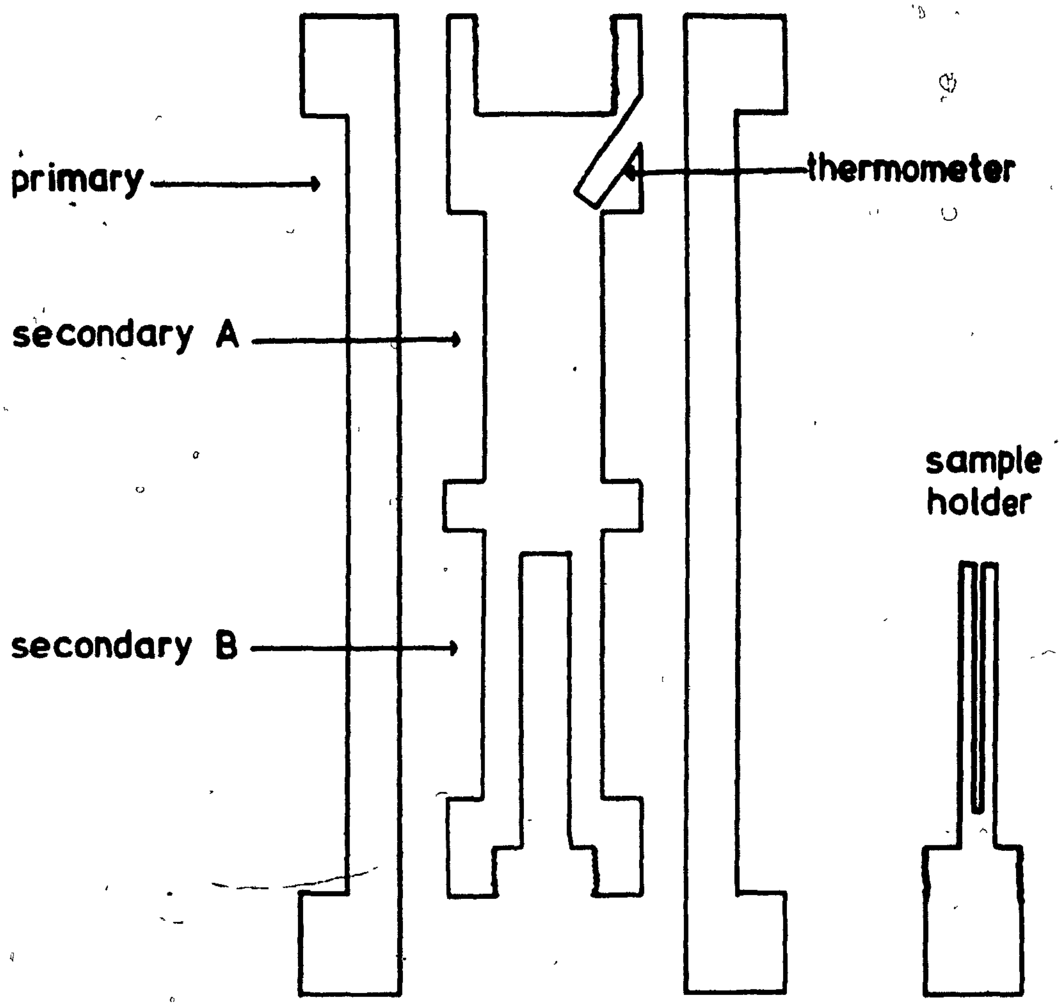

figure 2.6 Cross-section of the primary and secondary coils for the ac susceptibility bridge used to measure T_c

where N = number of turns per unit length

I = current

This is true assuming an infinitely long primary. In the present case the primary extends 5/8 inch beyond either secondary which are themselves 1 inch long. With these parameters the difference in H from one end to the other of one secondary is less than 10%, so the assumption is reasonable. The flux through one of the secondaries without the sample is:

$$\Phi = \int B \, da$$

Around one turn this is:

$$\Phi_1 = \mu_0 NIA$$

so that the total flux linkage between the primary and one secondary is:

$$\Phi = \mu_0 NIAnl$$

where A = cross sectional area of secondary

n = number of turns of secondary/unit length

l = length of secondary

thus $d\Phi/dt = V = \mu_0 \, N \, n \, A \, l \, dI/dt$

in the present case, where there are 3638 turns in the 3.5 inch primary and 6265 turns in the 1 inch secondary:

$$N = \frac{3638 \times 100}{3.5 \times 2.54}$$

$$n = \frac{6265 \times 100}{2.54}$$

$$A = \left(\frac{3}{16} \times 2.54 \times 10^{-2}\right)^2 \times \pi \ m^2$$

$$A = 7.12 \times 10^{-5}\ m^2$$

$$l = 2.54\times10^{-2}\ m$$

$$\frac{dI}{dt} = 1 \times 2\pi \times 37 \quad \text{where } f = 37 \text{ hz,}$$

The frequency f is chosen to avoid resonance with other frequencies in the laboratory. So without the sample the expected induced voltage across one of the secondaries is:

$$V = 5.35\ mV/mA$$

Now suppose that, due to the Meissner effect, flux is excluded from a volume Ω (the superconducting sample). The flux then becomes

$$\Phi = \mu_o NIAnl - \mu_o NIA_o nl_o$$

where $A_o l_o = \Omega_o$ = volume of sample

for a typical sample

mass = 2 mg

density = 7 g/cm^3

volume $\sim 3 \times 10^{-4}$cm^3

so the sensitivity is

$$\frac{\Delta V}{V} = \frac{\mu_o NInA_o l_o}{\mu_o NInAl}$$

$$= \frac{\Omega_o}{\Omega}\ \frac{\text{(sample)}}{\text{(sample holder)}}$$

$$= \frac{0.356\times10^{-3}\ cm^3}{1.81\times10^{-6}\ m^3}$$

$$\frac{\Delta V}{V} = 1.97\times10^{-4}$$

i.e. with the above assumptions, we should expect a fractional change of voltage across one coil of the astatic pair of about two parts in 10^4 when the sample becomes superconducting.

The signal from the two secondaries, one with the sample and the other without, was then connected to the input of a lock-in amplifier. Because it was not possible to balance the secondaries exactly and because of the presence of the sample there was always a slight out-of-balance signal at the output of the lock-in. To eliminate this signal an air-coil transformer was used to provide an additional variable linkage between the primary and secondary circuits, as shown in figure 2.5. The secondary of the air-coil transformer was connected in series with the signal and its amplitude varied by rotating it with respect to the primary. By this means a true null (to 5 parts in 1000) was obtained at the input of the lock-in amplifier. Furthermore since the two primaries were in series, fluctuations in current were unimportant to first order. This allowed a small change in $V_A - V_B$, the signal δV, to be detected by the lock-in amplifier when the magnetic flux originally present in the sample was ejected due to the sample becoming superconducting.

A fractional change of voltage across one coil of the astatic pair of one part in 10^4 resulted in the output signal of the lock-in amplifier δV to be of order 20 times larger than the noise. Two characteristic curves are shown in figure 2.7. The two curves shown have slightly different

figure 2.7 Two typical T_c curves for $Ni_{25}Zr_{75}$ as plotted by the X-Y recorder for the susceptibility bridge. Notice small differences in both the height of the transition and the onset (highest) temperature. a) $t_{anneal} = 20$ min b) $t_{anneal} = 2.5$ min

heights for two reasons. The samples for each curve have the same density but slightly different mass, so their volumes are slightly different. As the signal depends on the volume this is one cause of the difference. Another is that the samples could not be placed in exactly the same position and they were not ideal samples in that they were not perfectly flat. Since the flux was not distributed uniformly through the secondary and the samples were not placed in identical positions with respect to the flux a different amount of flux was ejected from each sample. This resulted in the two samples having slightly different signal heights. Because it was not possible to get an exactly reproducible signal height for a transition it was not possible to determine whether the whole sample went superconducting to better than about 10%.

The temperature was measured using a four-terminal germanium resistance thermometer calibrated against the vapour pressure of helium for temperatures below 4.265 K using published tables(2.4). The vapour pressure was measured using two highly sensitive mechanical gauges (Wallace & Tiernan) accurate to 0.01 mm Hg. With this thermometer the error on the individual T_c measurements was ± 0.005 K. The overall accuracy of the temperature measurements was verified against the T_c of standard samples of tin, indium, and the lambda point of helium. The measured T_c was consistently 0.02 K above the standard values.

2.5 Upper Critical Field (H_{c2}) and Susceptibility (χ) Measurements

Because of the unusual behaviour of their ~~critical~~ critical temperatures under annealing, Fe-Zr samples were further subjected to both upper critical field (H_{c2}) and susceptibility measurements. $\left(\frac{dH_{c2}}{dT}\right)_{T_c}$ was measured in order to find the density of electron states of the sample. This was measured using a standard four-terminal resistance measurement inside an induction magnet. T_c was found for a series of fields H, to a maximum of 45 KG, and the graph of H_{c2} vs T_c yielded $\left(\frac{dH_{c2}}{dT}\right)_{T_c}$.

Susceptibility measurements were then performed to determine the effect of annealing on the magnetic properties of Fe-Zr. Measurements of χ were performed using a Faraday force balance using Lewis gradient coils to generate the necessary field gradient$^{(2.5)}$. The balance was automated in the laboratory$^{(2.6)}$ using an IBM Personal Computer. A sample of approximately 30 mg resulted in a signal 4 times larger than the sample holder, with an error of 2%.

Both H_{c2} and χ measurements were performed on Fe-Zr samples. The samples were subsequently annealed and the measurements repeated. The same samples were used so as not to introduce possible inhomogeneities of the sample into the calculations. Thus the effect of annealing on some magnetic properties related to superconductivity in Zr based metallic glasses were determined.

Chapter 3 - Results

3.1 Irreversible Relaxation

The objective of the first part of this work was to compare the effects of annealing on the superconducting transition temperature, T_c, of $X_{25}Zr_{75}$ where X = Fe, Co, Ni, Cu. 75% zirconium was chosen because at that composition the four glasses had T_c attainable within the temperature range of pumped liquid helium.

The superconducting transition temperature was measured using the ac susceptibility bridge described in Chapter 2. T_c was measured for all as-quenched samples. For $Co_{25}Zr_{75}$, $Ni_{25}Zr_{75}$ and $Cu_{25}Zr_{75}$ different pieces of the same ribbons were annealed at 488 K in the Differential Scanning Calorimeter for varying periods of time not exceeding three hours or in the horizontal furnace for longer times, and T_c subsequently measured. All samples were two cm long. The annealing procedures are described in more detail in Chapter 2. Different pieces of the ribbons were used instead of successively annealing the same piece because the ribbons were believed to be fairly homogeneous and T_c in these samples does not change appreciably over small composition changes about 75% zirconium(3.1). This was confirmed when different pieces of the same ribbon were measured and found to have the same T_c, so the procedure was reasonable.

For $Fe_{25}Zr_{75}$ this was not the case. T_c changes considerably with very small changes in composition(3.1), so it is possible that changes due to annealing may be masked by small fluctuations in concentration. This was shown by an identical series of anneals performed on different samples and compared with results obtained on one sample annealed sequentially. The data from different samples showed slightly more scatter (see figure 3.1); thus for Fe-Zr a single sample sequentially annealed was used for each series of measurements. The sequence of anneal times extended from 1 minute to 16 days in a logarithmic scale: 1 min, 2 min, ..., 8 days, 16 days, the total annealing time being taken as the cumulative time.

Graphs of log t_{anneal} vs T_c for $Fe_{25}Zr_{75}$, $Co_{25}Zr_{75}$, $Ni_{25}Zr_{75}$ and $Cu_{25}Zr_{75}$ are shown in figures 3.1, 3.2, 3.3, and 3.4 respectively for an anneal temperature of 488 K. In the graphs both similarities and differences are seen between the different alloys. One similarity among the alloys is that there is a large change in T_c between the as quenched glasses and those annealed for only one minute. This large change was found in all the systems examined, and is discussed in Chapter 4. Another similarity is that for the anneals between 1 and 1000 minutes T_c changes roughly logarithmically with time annealed, although there is a difference in the slopes of the curves. The slopes range from 17 log(min)/K for $Fe_{25}Zr_{75}$ to -33 log(min)/K for $Co_{25}Zr_{75}$, to -26 log(min)/K for $Ni_{25}Zr_{75}$, and -19 log(min)/K for $Cu_{25}Zr_{75}$. This suggests a larger depression of T_c with increased valence of the 3d transition element in the alloy. A surprising result is that for $Fe_{25}Zr_{75}$ T_c initially increases on

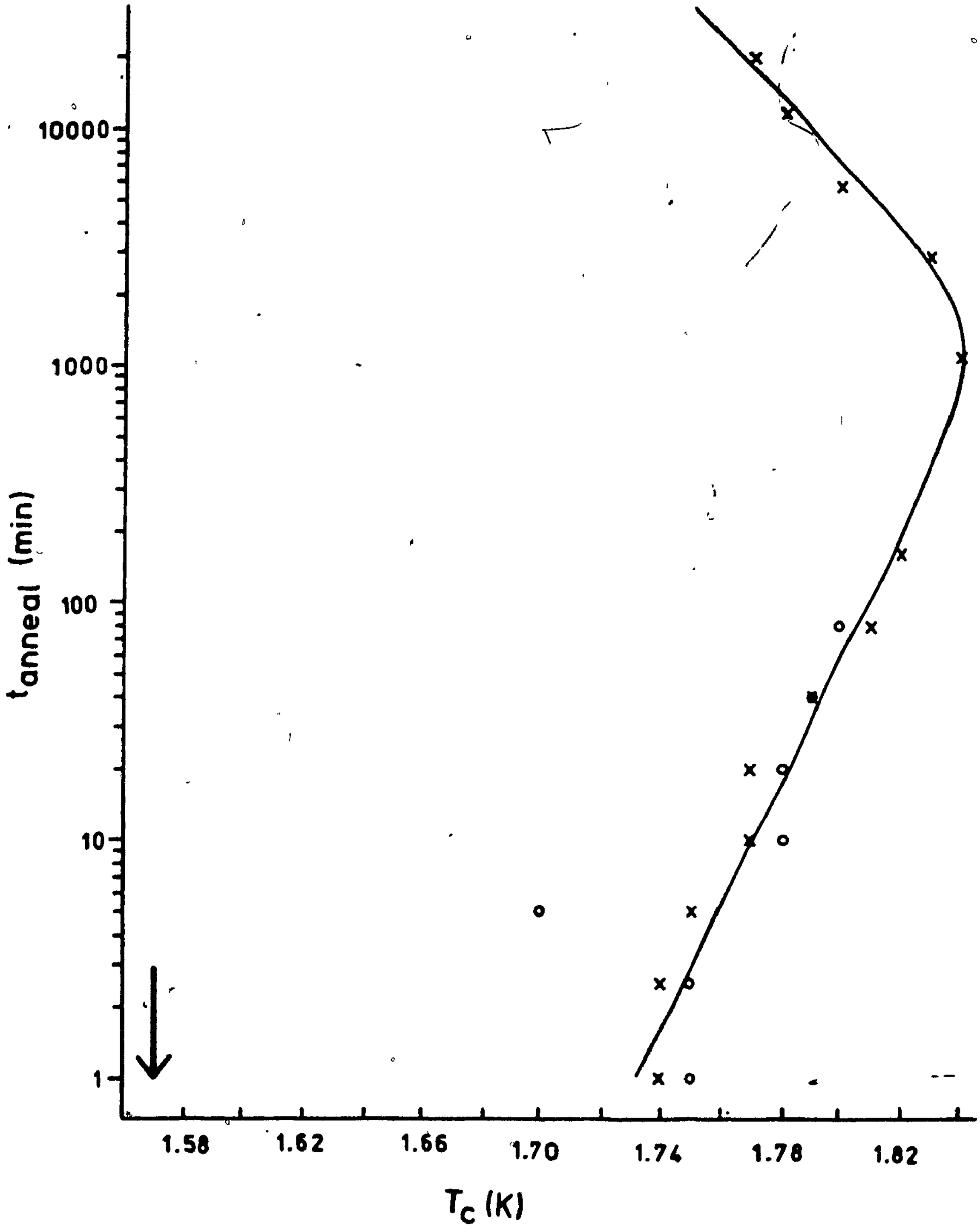

figure 3.1 Graph of log t_{anneal} vs T_c for $Fe_{25}Zr_{75}$ #2. The arrow indicates the as quenched T_c.

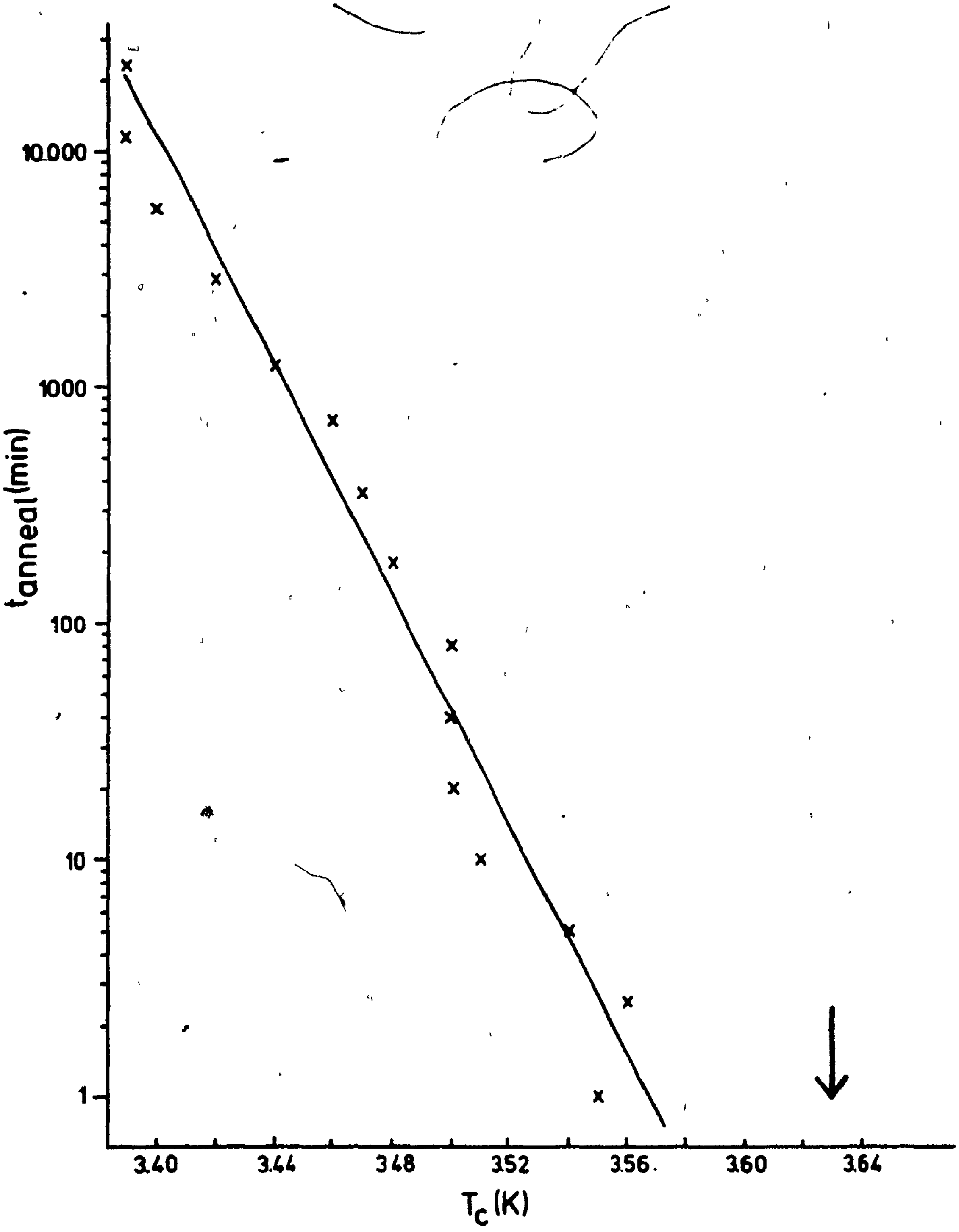

figure 3.2 Graph of log t_{anneal} vs T_c for $Co_{25}Zr_{75}$. The arrow indicates the as quenched T_c.

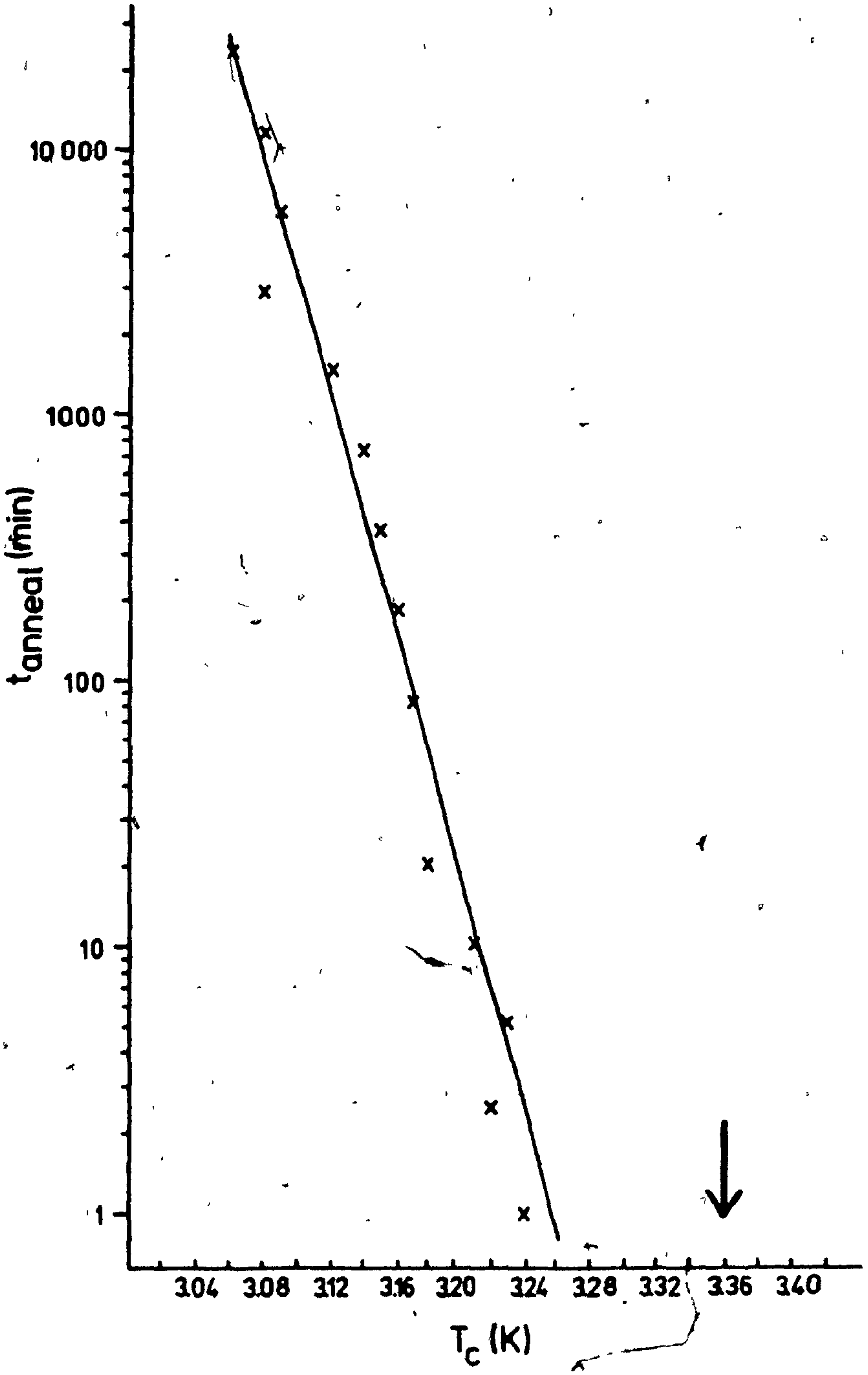

figure 3.3 Graph of log t_{anneal} vs T_c for $Ni_{25}Zr_{75}$. The arrow indicates the as quenched T_c.

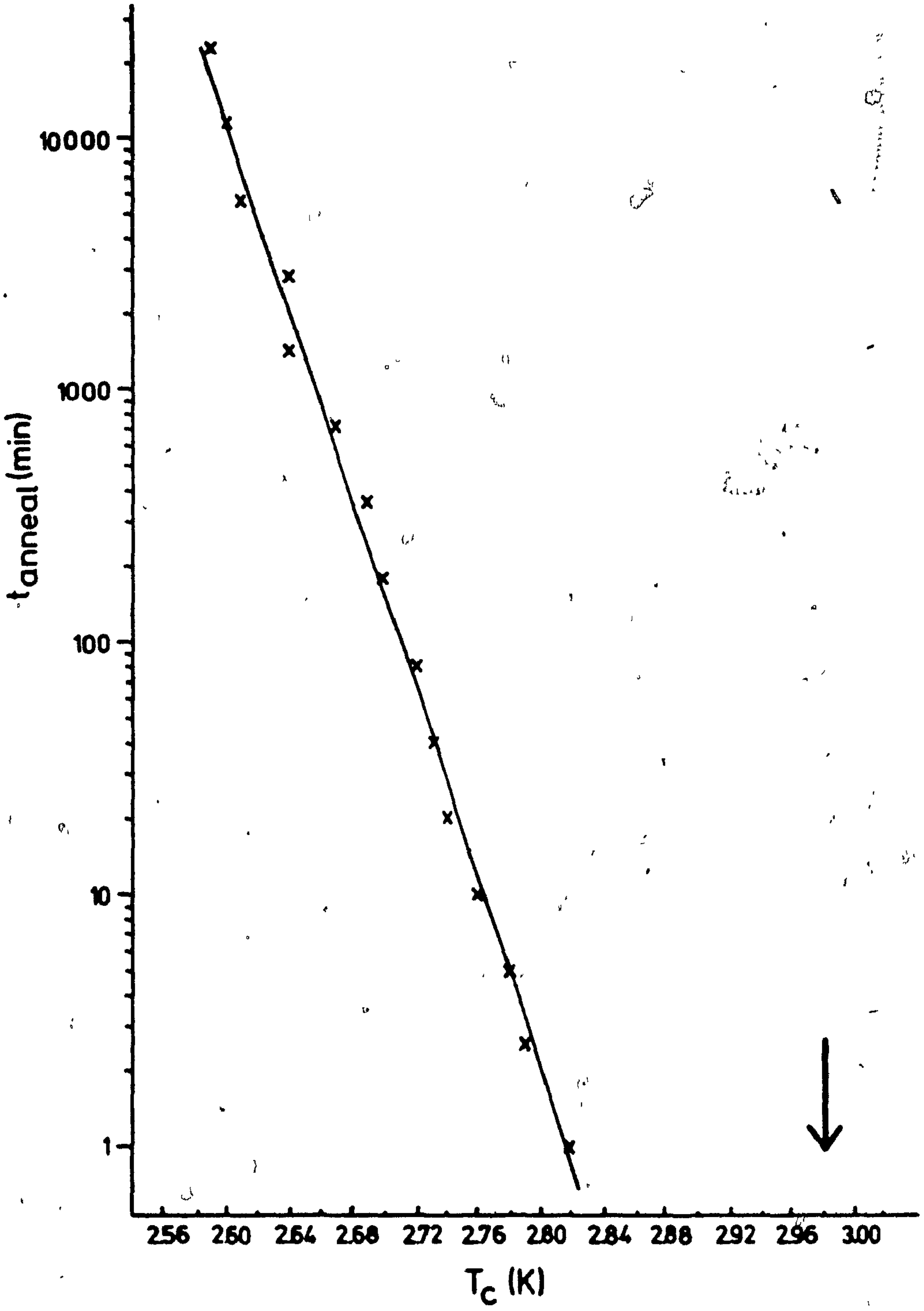

figure 3.4 Graph of log t_{anneal} vs T_c fo~~r Cu~~$_{25}$~~Zr~~$_{75}$. The arrow indicates the as quenched T_c.

annealing! All previously reported experiments have found that annealed glasses have lower T_c than the corresponding as quenched glasses$^{(3.2)}$.

Another similarity is that T_c does not show any sign of reaching an equilibrium value but continues to change continuously through to the longest anneal of 16 days. The exception to this is Fe-Zr which changes from increasing with anneal time to decreasing with anneal time, but it still exhibits no tendency to saturate. This result is somewhat surprising as it had been supposed$^{(3.2)}$ that metallic glasses have a decrease in T_c with low anneal temperature until T_c reaches a lower limit at which it saturates until crystallization.

3.1.1 Fe-Zr system

Fe-Zr was examined in the range of 75-80% zirconium. For the Fe-Zr system, the superconducting transition temperature T_c is very sensitive to composition and for larger iron concentration (and lower T_c) the superconducting state was not detectable on the ac susceptibility bridge within the accessable temperature range (ie. $\geq$ 1K). Since the measurements performed on this system were to observe changes due to iron, the iron content was kept as large as possible. Given the constraints on composition, the iron concentration was held in the range of 20-25%. The actual percentage of Fe and Zr in the samples was determined using an electron microprobe and by comparing results of both T_c and crystallization temperatures, T_x, to published data. The results are summarized in table 3.1 where samples are identified by date of manufacture.

Table 3.1

Fe concentration for Fe-Zr samples

sample	Fe concentration			
	nominal	from T_x^*	from $T_c^\dagger$	microprobe
22jan86	20	17.6	20.98	20.7
18nov85	20	....	23.15	20.4
29mar84	22.5	18.9	23.57	23.7
14jun85	25	27.3	25.95	26.3
25mar86	25	....	25.68	26.0

* ref. 3.3

† ref.3.1

Note that the values of concentration obtained from T_x are not consistent with the other values. This is because T_x is sensitive to changes in conditions other than composition, and, as external factors are not likely to have been the same for the various samples, this is not expected to be a precise indicator of the composition. Results from T_c and microprobe agree reasonably well for all samples except 18nov85. For this the result from T_c was higher than expected, possibly due to annealing at the time of manufacture, which is discussed later. Except for this sample, the composition is believed to be roughly that indicated by T_c measurements. For simplicity the samples are refered to by their nominal composition: 22jan86 is refered to as $Fe_{20}Zr_{80}$ #1; 18nov85 as $Fe_{20}Zr_{80}$ #2; 29mar84 as $Fe_{22.5}Zr_{77.5}$ and 25mar86 is refered to as $Fe_{25}Zr_{75}$. Where 14jun85 is used it is refered to as $Fe_{25}Zr_{75}$ #2.

Because of their unusual behaviour on annealing, changes in T_c of annealed samples of the Fe-Zr system were examined for a fuller understanding of the processes involved leading to the increase in T_c. Graphs of log t_{anneal} vs T_c of $Fe_{20}Zr_{80}$ #1, $Fe_{20}Zr_{80}$ #2, $Fe_{22.5}Zr_{77.5}$, and $Fe_{25}Zr_{75}$ #2 are shown in figure 3.5. T_c in annealed samples rises as much as 0.10 K above that of the as quenched samples and reaches a maximum value at between 10 and 1000 minutes at an anneal temperature of 488 K. For longer anneal times T_c decreases.

One possible explanation for the abrupt change in slope is that it is related to the onset of crystallization. X-ray analysis performed on a 1.56 mg $Fe_{25}Zr_{75}$ sample that had been annealed at 488 K for a total of 16 days, the longest anneal time, did not show any evidence of crystallization. But we know that T_c is a very sensitive characteristic of a glass and can be expected to change with less than 2% crystallization, the approximate resolution of the X-ray diffractometer. It is therefore necessary to predict the corresponding change in T_c for this minimum amount of crystallization. 2% crystallization of ω-Zr in

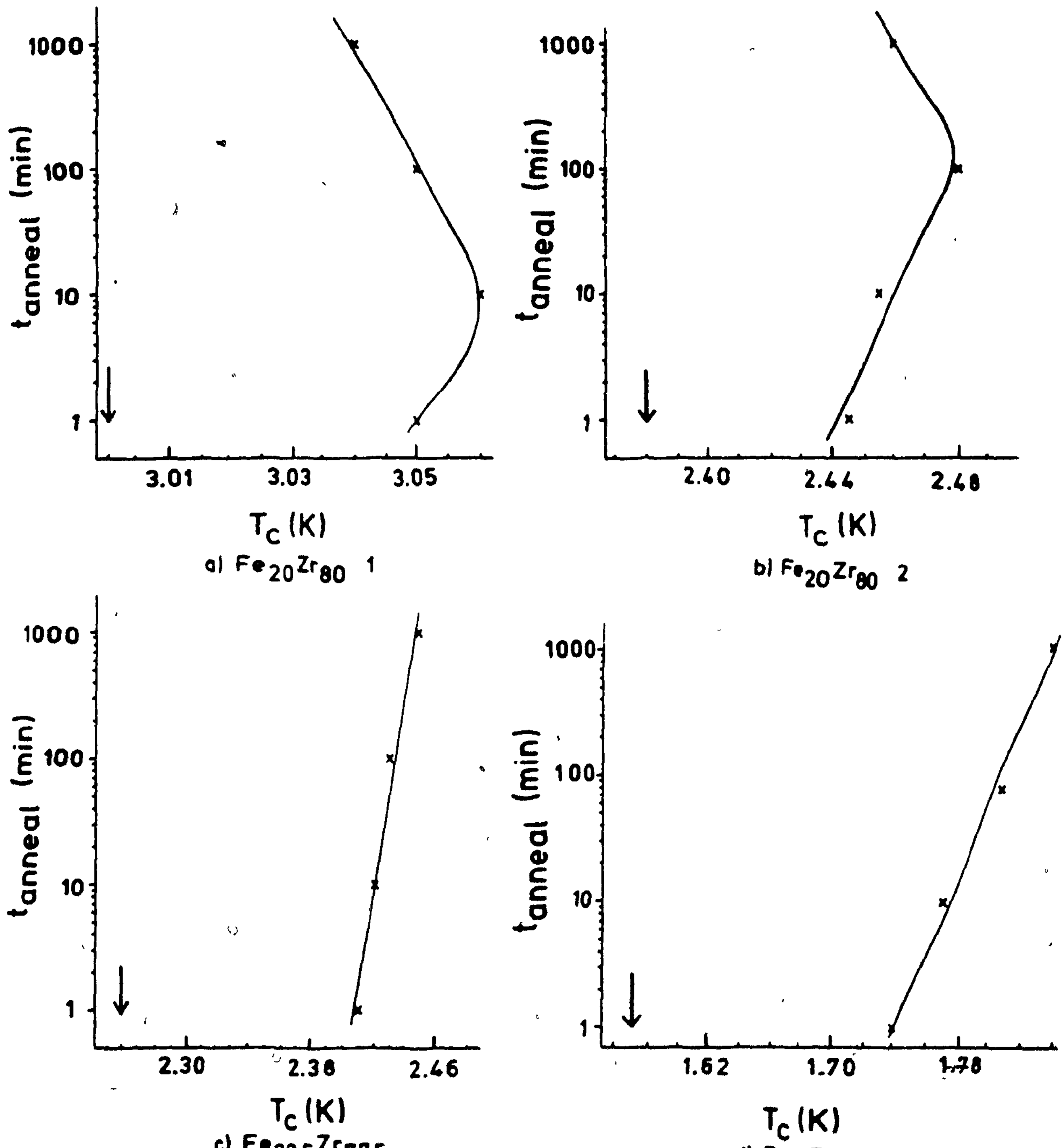

a) $Fe_{20}Zr_{80}$ 1

b) $Fe_{20}Zr_{80}$ 2

c) $Fe_{22.5}Zr_{77.5}$

d) $Fe_{25}Zr_{75}$

figure 3.5 Graphs of log t_{anneal} vs T_c for a) $Fe_{20}Zr_{80}$ #1, b) $Fe_{20}Zr_{80}$ #2, c) $Fe_{22.5}Zr_{77.5}$, d) $Fe_{25}Zr_{75}$ #2. The arrows indicate the as quenched T_c.

$Fe_{25}Zr_{75}$, providing that there are no other crystallization products, corresponds to an increase in Fe concentration in the remaining amorphous matrix of 0.51 at% which, from published data(3.1), corresponds to a drop in T_c of 0.15 K. After an anneal of 16 days, the longest anneal performed, the drop in T_c was only 0.07 K from the maximum value. This corresponds to 1.0% crystallization of ω-Zr so, assuming no other crystallization products, we did not expect to be able to detect any crystallization on the X-ray powder diffractometer. The evidence is inconclusive, but, because of other evidence described later, we do not believe that crystallization has occured at this stage.

Besides crystallization of ω-Zr there could also be some crystallization of $FeZr_2$ or $FeZr_3$(3.3). But the time for crystallization of these can be estimated from the Arrhenius relation $t_x = t_o \exp\left(E_a/kT\right)$; the constants t_o and E_a are found from DSC measurements of t_x for a given T. However, such data predicts crystallization occuring on the order of years, not days, at an anneal temperature of 488 K. So crystallization of $FeZr_2$ or $FeZr_3$ is not likely, and there is no direct evidence of crystallization of ω-Zr. Thus we conclude that the change in behaviour is more likely due to a fundamental change in the glass, as will be discussed in Chapter 4.

Another point of interest is the slope of the curves. The slope ranges from 17 log(min)/K for $Fe_{25}Zr_{75}$ to ~25 log(min)/K for $Fe_{20}Zr_{80}$ #1. T_c increases upon annealing for $Fe_{20}Zr_{80}$, more for $Fe_{22.5}Zr_{77.5}$, and again more for $Fe_{25}Zr_{75}$, suggesting that the increase in T_c upon annealing is a function of Fe concentration. These results are also discussed in Chapter 4.

Both the susceptibility χ and the upper critical field H_{c2} were also measured in order to obtain information about the density of electron states at the Fermi energy. The relationship between these two parameters and the density of states will be discussed in Chapter 4. The measurements were performed in order to determine the interactions responsible for the behaviour of T_c.

χ was measured several times at room temperature for samples of approximately 30 mg of each alloy. For a better estimate of the error inherent in the measurements the sample was removed from the sample holder and then replaced before being remeasured. The susceptibility was calculated from the slope of a curve of M vs H using a linear least squares fit to 95% confidence. A typical fit is shown in figure 3.6. Individual measurements had error less than 4%, and the variation within measurements of the same sample was less than ± 2%. Comparing the as quenched susceptibilities there was a measureable increase in χ with increase in Fe concentration, the values of χ ranging from 2.13×10^{-6} emu/g for $Fe_{20}Zr_{80}$ to 2.53×10^{-6} emu/g for $Fe_{25}Zr_{75}$. The samples were annealed in the furnace described in Chapter 2 at 488 K for 500 minutes and then the susceptibility was remeasured. The susceptibility of each sample decreased after annealing to values ranging from 2.01×10^{-6} emu/g for

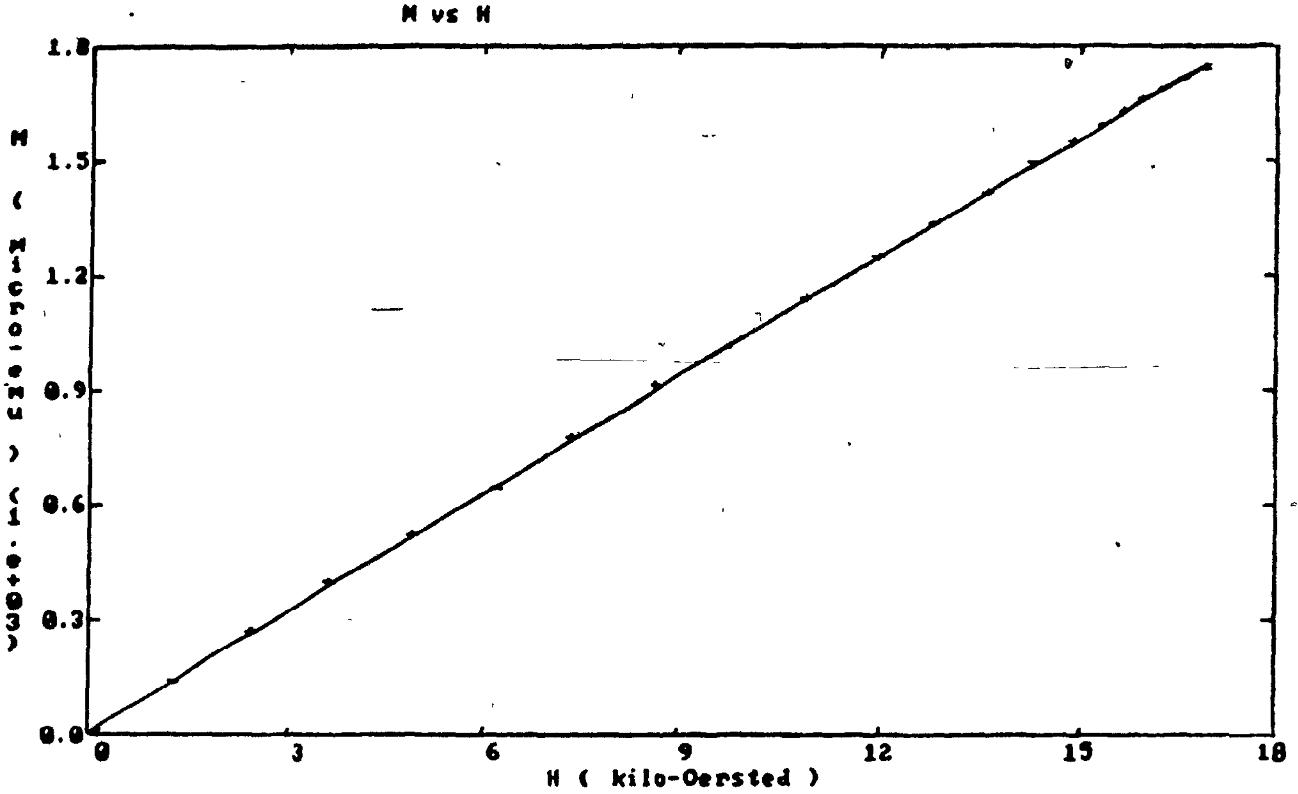

figure 3.6 Magnetism against field for $Fe_{25}Zr_{75}$ after subtracting the sample holder

$Fe_{20}Zr_{80}$ to 2.39×10^{-6} emu/g for $Fe_{25}Zr_{75}$. This represents a decrease in χ ranging from 5% for $Fe_{20}Zr_{80}$ #2 to 16% for $Fe_{22.5}Zr_{77.5}$. A list of χ for as quenched and annealed samples is given in table 3.2.

The upper critical field H_{c2} of as quenched and annealed samples was measured as described in Chapter 2. To find $\left(\frac{dH_{c2}}{dT}\right)_{T_c}$ T_c was measured using a four point resistance probe for varying applied fields. Curves of upper critical field vs T_c were linear for applied fields not exceeding 26.5 KOe for $Fe_{1-x}Zr_x$, x = 80, 77.5, 75. The slope of the linear part of the curve of H_{c2} vs T_c gave $\left(\frac{dH_{c2}}{dT}\right)_{T_c}$. This varied from -33.8 ± 1.0 KOe/K for $Fe_{20}Zr_{80}$ to -36.8 ± 1.0 KOe/K for $Fe_{25}Zr_{75}$, as shown in figures 3.7-3.10. Estimates of the error were obtained by estimating the largest possible difference in slope for a set of points. The error was consistently ± 1.0 for the slopes of upper critical field measurements. Within the error it is possible to detect changes in slope with annealing, but the error is large compared to the changes, making the latter only just resolvable (see table 3.2). When the samples were annealed the increment in slope varied from 5% for $Fe_{20}Zr_{80}$ #1 to 12% for $Fe_{22.5}Zr_{77.5}$. In order to compare results with a non-ferromagnetic glass, similar measurements were performed on the sample $Ni_{25}Zr_{75}$. For this sample $\left(\frac{dH_{c2}}{dT}\right)_{T_c}$ increased from -31.1 ± 1.0 KOe/K to -27.4 ± 1.0 KOe/K upon annealing. A list of $\left(\frac{dH_{c2}}{dT}\right)_{T_c}$ for as quenched and annealed samples is

Table 3.2

Measured values of χ and $\left(\frac{dH_{c2}}{dT}\right)_{T_c}$ for as quenched and annealed samples of Fe-Zr

sample	as quenched χ $(\times 10^{-6}$emu/g)	 $\left(\frac{dH_{c2}}{dT}\right)_{T_c}$ KG/K	annealed χ $(\times 10^{-6}$emu/g)	 $\left(\frac{dH_{c2}}{dT}\right)_{T_c}$ KG/K
$Fe_{20}Zr_{80}$ #1	2.13±0.1	-33.8±1.0	2.01±0.1	-32.1±1.0
$Fe_{20}Zr_{80}$ #2	2.21	-35.3	2.11	-32.3
$Fe_{22.5}Zr_{77.5}$	2.47	-34.6	2.07	-30.5
$Fe_{25}Zr_{75}$	2.53	-36.8	2.39	-34.2

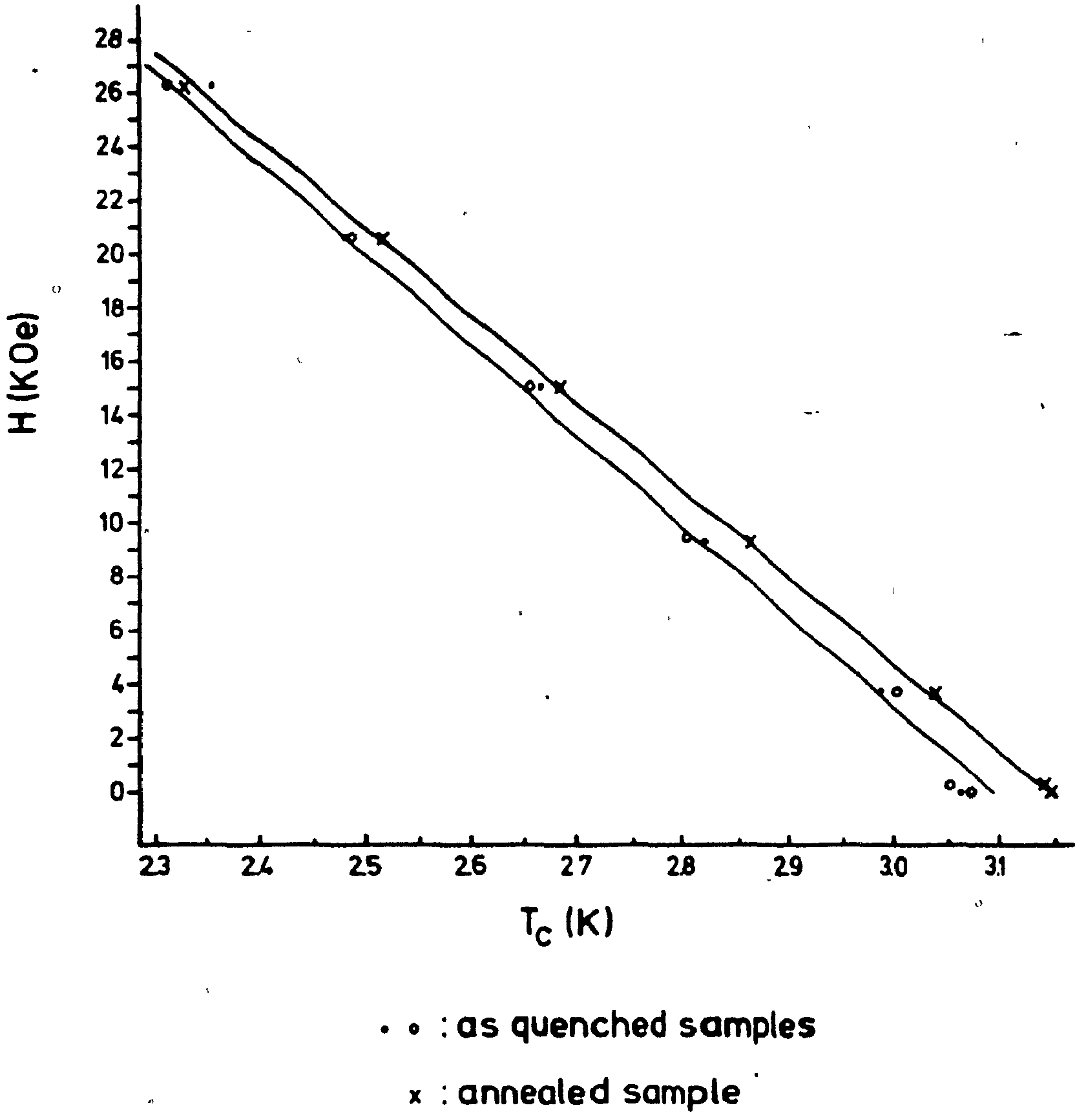

figure 3.7 Graph of $\left(\frac{dH_{c2}}{dT}\right)_{T_c}$ for $Fe_{20}Zr_{80}$ #1.

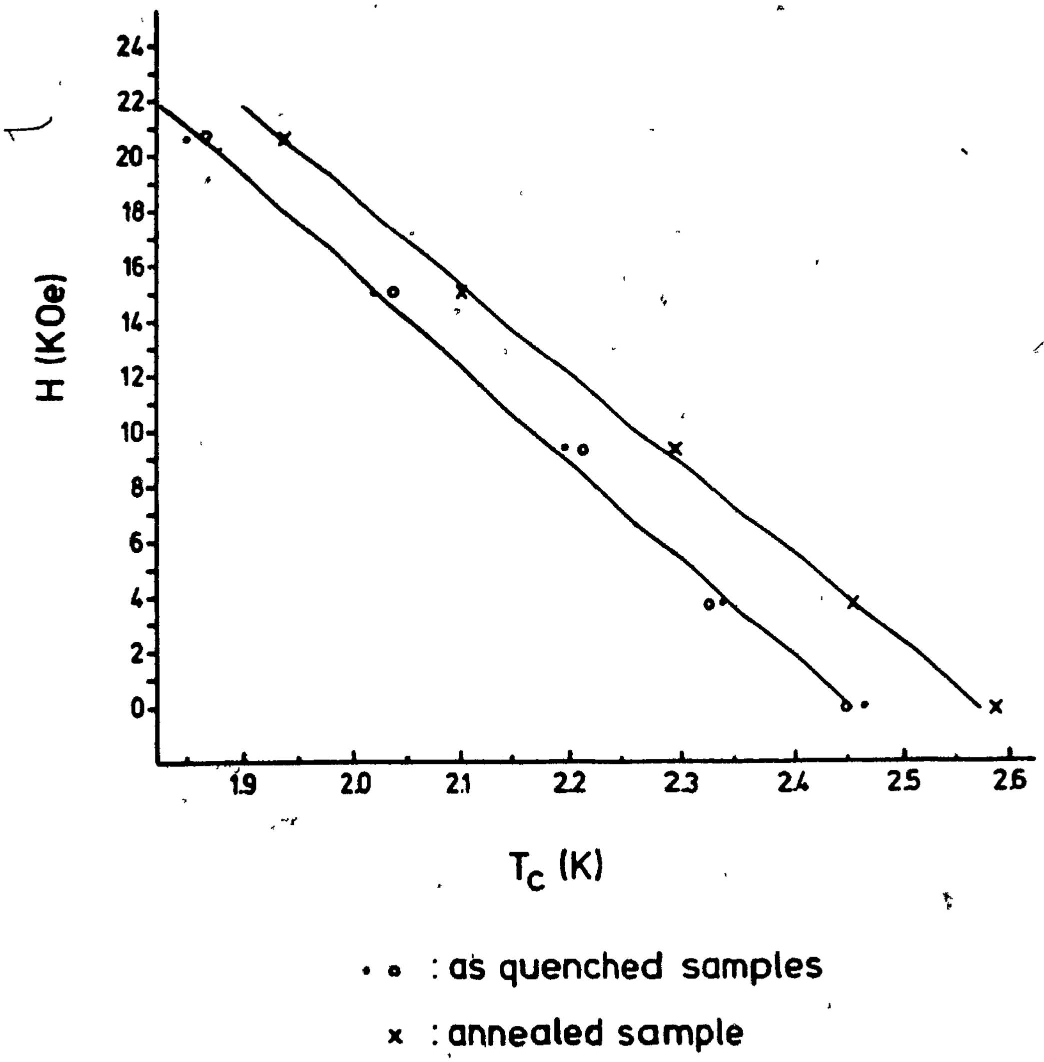

figure 3.8 Graph of $\left(\frac{dH_{c2}}{dT}\right)_{T_c}$ for $Fe_{20}Zr_{80}$ #2.

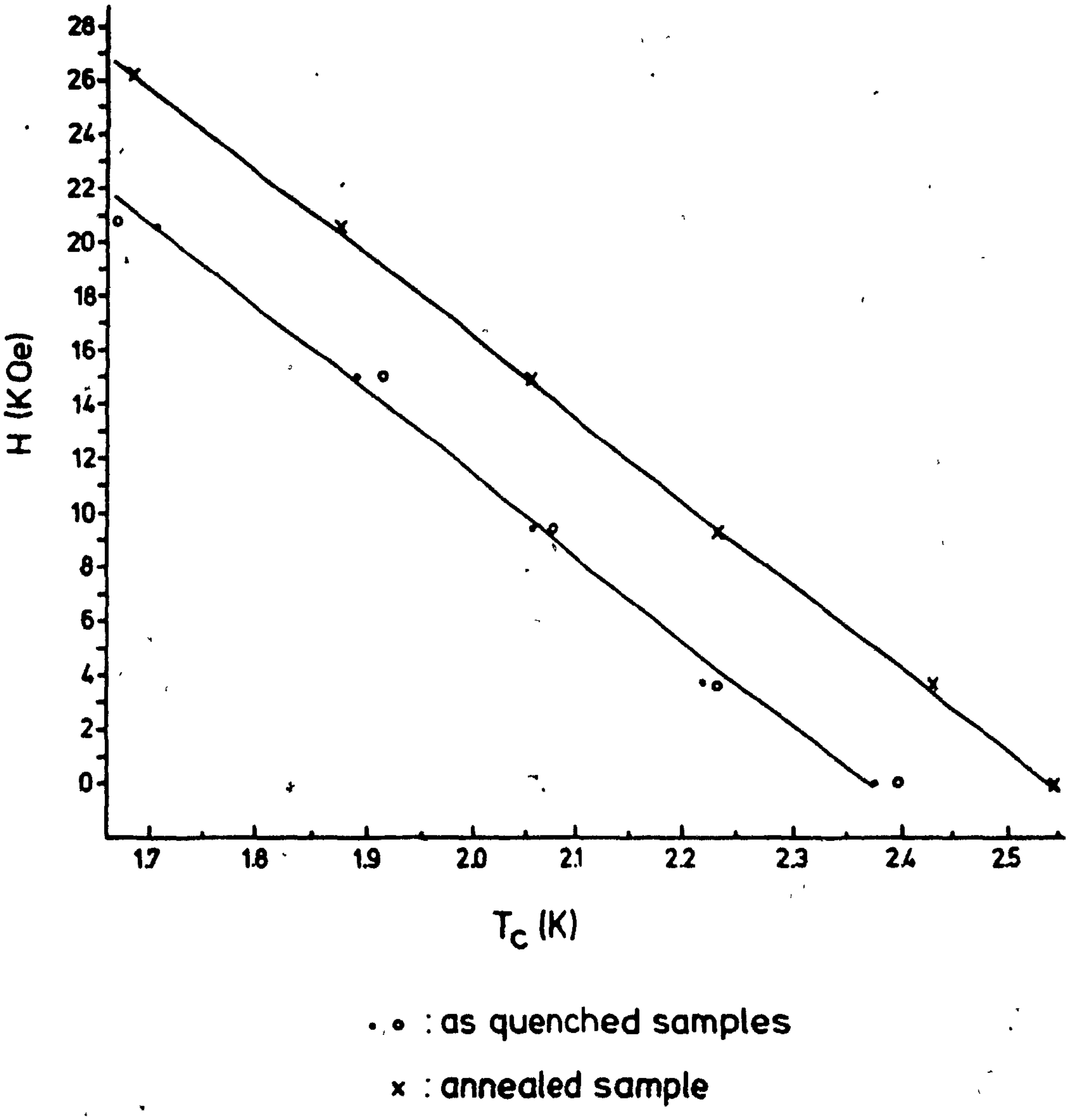

figure 3.9 Graph of $\left(\frac{dH_{c2}}{dT}\right)_{T_c}$ for $Fe_{22.5}Zr_{77.5}$.

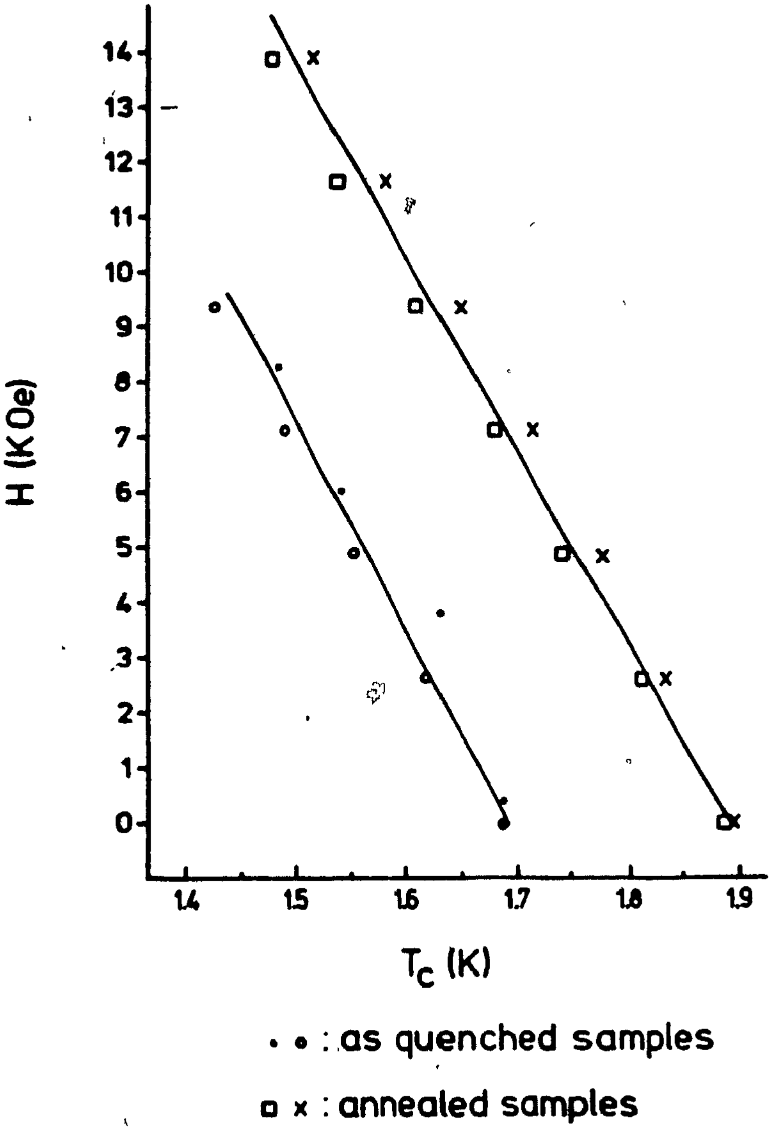

figure 3.10 Graph of $\left(\frac{dH_{c2}}{dT}\right)_{T_c}$ for $Fe_{25}Zr_{75}$.

given in table 3.2. Using these measurements of χ and H_{c2} it is possible to deduce the magnitudes of both the electron-phonon and spin-fluctuation interactions, as will be discussed in Chapter 4.

3.2 Reversible Relaxation

The third part of this work involved the reversible component of relaxation. A number of systems, both binary and ternary, were examined, specifically the systems $X_{33}Zr_{67}$ (X = Ni, (CuNi), Cu), $X_{25}Zr_{75}$ (X = Fe, Co, Ni), and $Ni_{24}Zr_{76}$.

Each alloy was annealed at 543 K for 1 hour and then annealed successively at constant increments of temperature starting at 398 K for 10 minutes at each new anneal temperature. T_c was measured after each anneal using the ac susceptibility bridge described in Chapter 2, and was found to vary very little. Above an anneal temperature of 543 K T_c did rise by a small amount for the samples $Ni_{24}Zr_{76}$ and $X_{33}Zr_{67}$ (X = Ni, (CuNi), Cu). A typical plot of T_c vs anneal temperature is shown in figure 3.11. Because of the temperature increase at this point the anneal temperatures just before the rise and at the top of the rise were chosen to test for the reversible component of relaxation. Neither $Fe_{25}Zr_{75}$ nor $Co_{25}Zr_{75}$ displayed this behaviour, as shown in figure 3.12 so they were not tested further for reversible effects. To test for reversible effects the samples were annealed sequentially to the higher of the two chosen

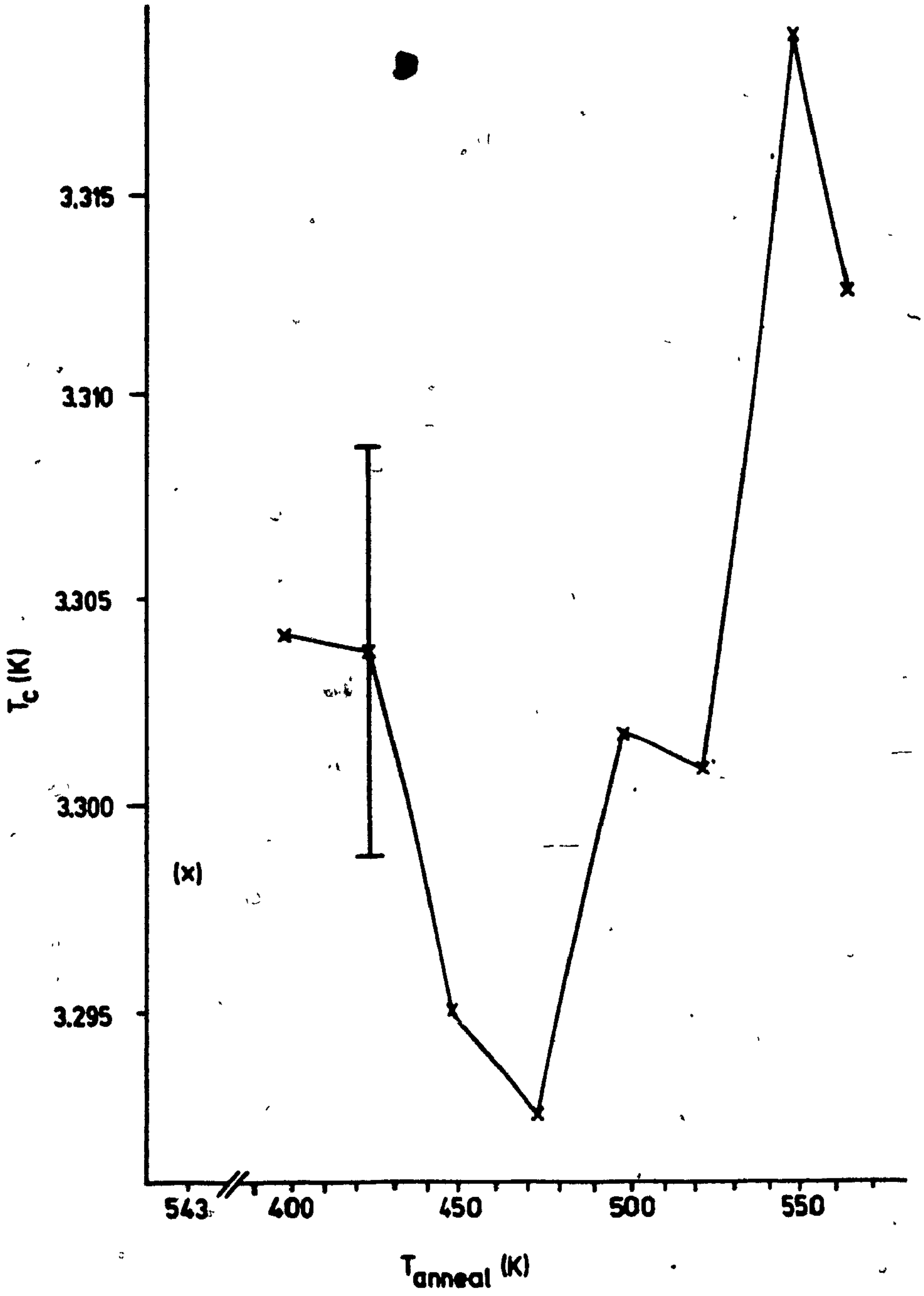

figure 3.11 T_c against t_{anneal} for a series of anneal temperatures with a representative error bar for $Ni_{24}Zr_{76}$, showing a small rise in T_c for anneals above 543 K.

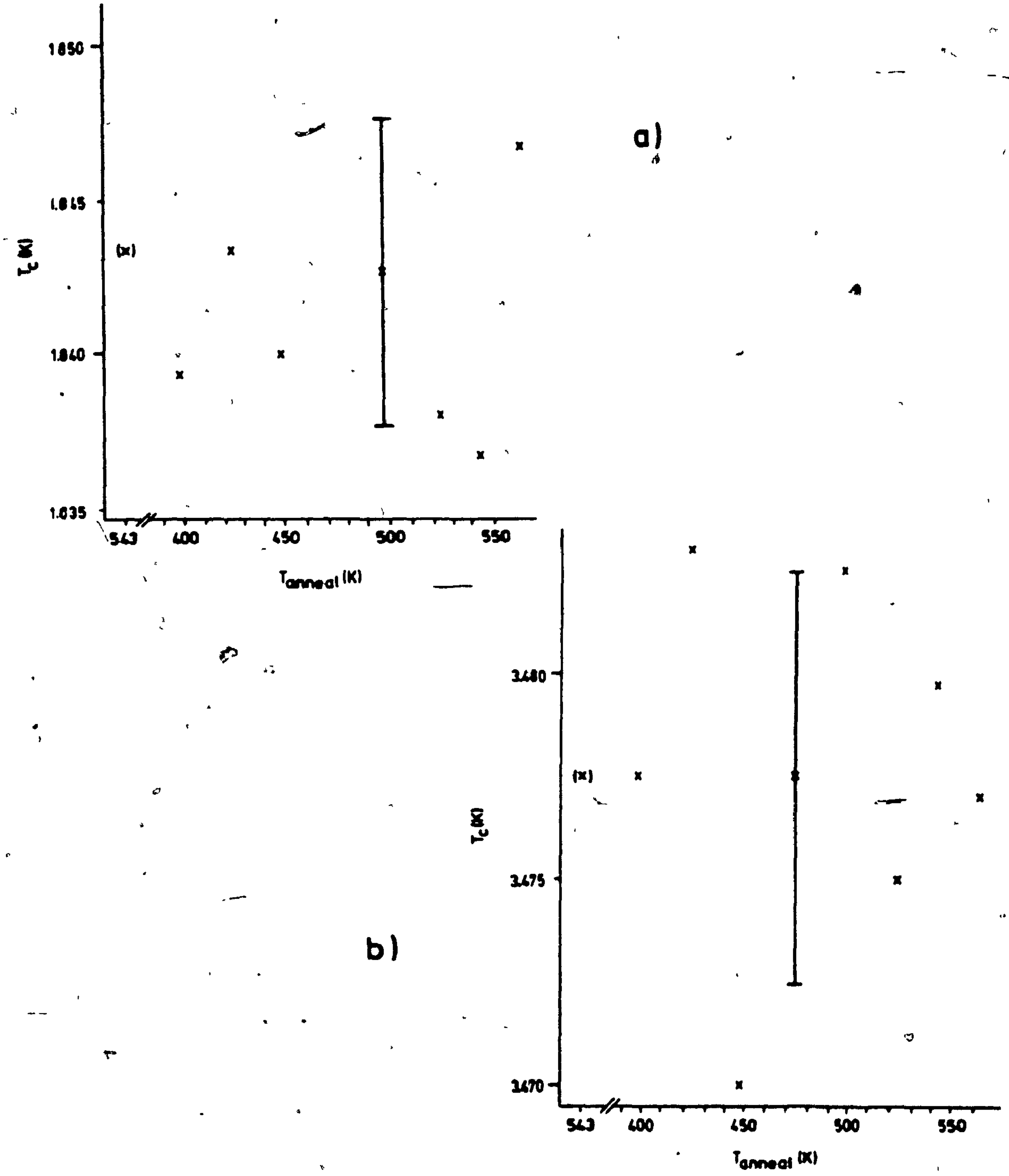

figure 3.12 T_c against t_{anneal} for a series of anneal temperatures with representative error bars for a) $Fe_{25}Zr_{75}$ and b) $Co_{25}Zr_{75}$, showing no systematic change in T_c.

temperatures, typically 563 K, followed by alternating anneals at the lower (typically 473 K) and higher temperatures. T_c was measured after each anneal. When Ni-Zr and Cu-Zr were tested in this manner they showed signs of reversible relaxation, though the effect was only just larger than the error in T_c. $Ni_{24}Zr_{76}$ showed the largest effect while $Ni_{33}Zr_{67}$ and $Cu_{33}Zr_{67}$ showed a very small effect and $(CuNi)_{33}Zr_{67}$ showed none at all. The results for Ni-, Cu-, and (CuNi)-Zr are shown in figure 3.13 for comparison. These results are discussed in Chapter 4.

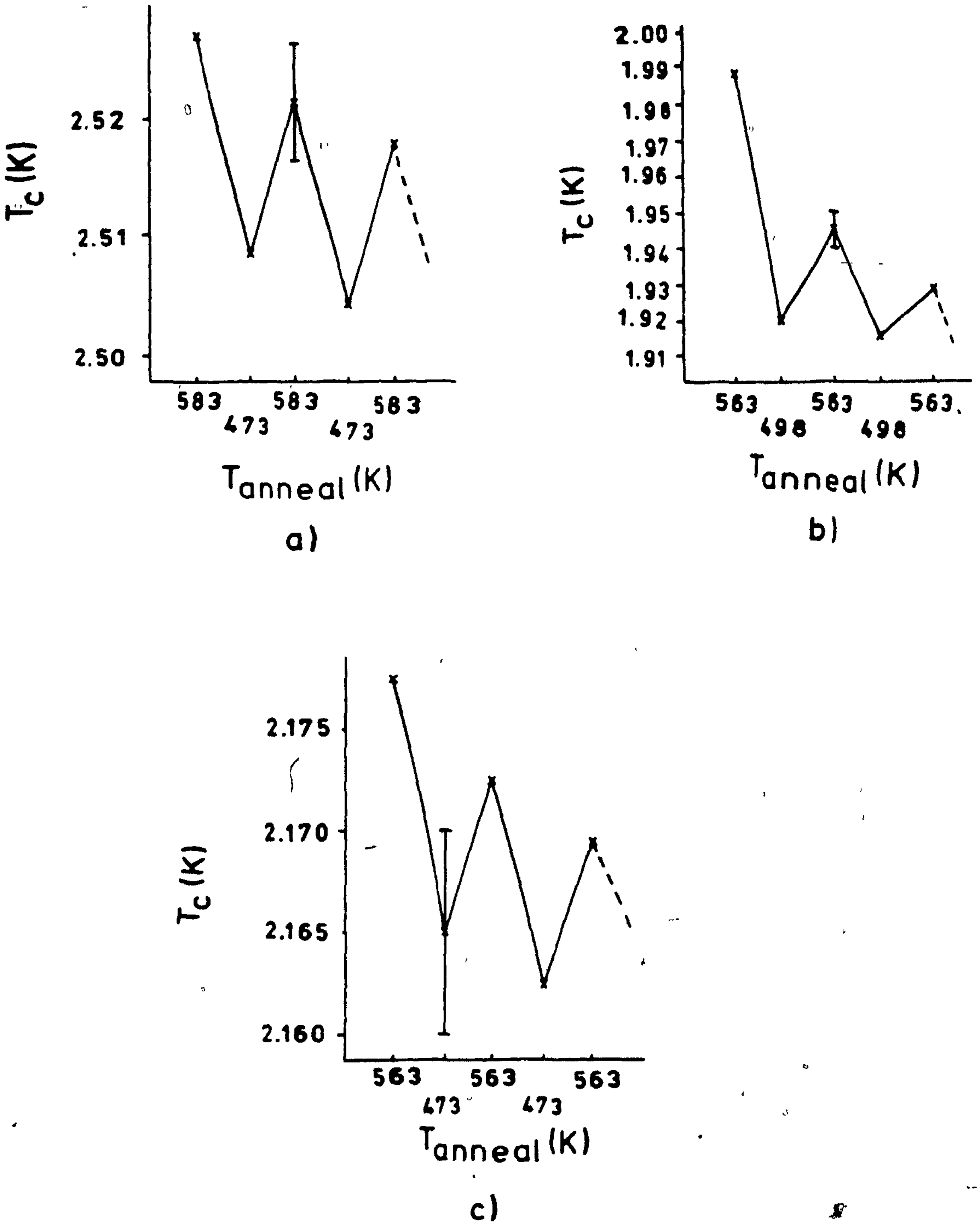

figure 3.13 T_c against t_{anneal} for a series of anneal temperatures with representative error bars for a) $Ni_{33}Zr_{67}$, b) $Cu_{33}Zr_{67}$, and c) $(CuNi)_{33}Zr_{67}$

Chapter 4 - Discussion

4.1 Irreversible Relaxation: Time Dependence

As observed in Chapter 3, T_c varies logarithmically with anneal time in the systems examined. The logarithmic anneal time dependence may be interpreted as a result of relaxation processes whose activation energies Δ are distributed over a wide range of energies. If we assume that the distribution of relaxation processes, $n(\Delta)$, is constant over some range of Δ and that the transition rate for one process varies as $\sim \omega_o e^{-(\Delta/T)}$, where ω_o is some characteristic atomic vibration frequency then the rate of change of n is given by:

$$\frac{dn}{dt} = -n\omega_o e^{-(\Delta/T)} \qquad (4.1)$$

Integration with respect to t yields

$$n(\Delta,t) = \exp\left[-\omega_o t \exp(-\frac{\Delta}{T})\right] \qquad (4.2)$$

The total number of relaxation processes which have occured after time t is given by

$$N(t) = \int n(\Delta,t)d\Delta \qquad (4.3)$$

Because of the double exponential dependence of $n(\Delta,t)$, the upper limit of the integral is effectively $\Delta = T \ln\omega_o t$, so to first order $N(t) \sim \ln t$. Assuming that T_c varies linearly with $N(t)$, then $T_c \sim \ln t$, as observed.

A similarity among the $X_{25}Zr_{75}$ (X = Fe, Co, Ni, Cu) alloys is, as discussed in Chapter 3, that there is a large change in T_c between as quenched glasses and those annealed for one minute. This large change was found in all systems examined. Assuming that the curve of log t_{anneal} vs T_c continues to be linear at smaller anneal times then we find that T_c for the as quenched samples corresponds to an anneal time on the order of 10^{-3} to 10^{-4} minutes, which is on the order of the time scale of the quench time. The time scale of relaxation is thus such that while the samples are being quenched from the melt they undergo preliminary relaxation. The relevance of this calculated time scale could be verified by looking for changes in as quenched alloys for various quench rates and when flash-annealed for times on the order of a few milliseconds. It certainly indicates that preliminary changes in the atomic order occur within the samples on a time scale much smaller that 1 minute.

The fact that T_c for Fe-Zr changes logarithmically with anneal time is further support for the dominant process to be relaxation, as opposed to crystallization, since changes in T_c due to crystallization should not be linear on a logarithmic time scale(4.1). The specific features of the curves of anneal time vs T_c are discussed later.

4.2 Irreversible Relaxation: Changes in Parameters of Superconductivity

Much work has been done to examine a variety of parameters relating to the superconducting transition temperature T_c for various metallic glasses.

Previous studies have examined the compositional dependence of T_c. Specific alloys examined include Cu-Zr(4.2)(4.3), Ni-Zr(4.4)(4.5), Co-Zr(4.5), and Fe-Zr(4.4). T_c has been examined by both low temperature specific heat and resistance measurements. In all of the alloys there is a significant drop in T_c with a decrease in the concentration of zirconium. The decrease in T_c with concentration varies regularly with the 3d element; this is illustrated by the fact that in Fe-Zr superconductivity disappears below ~ 70 at% Zr while in Cu-Zr it only disappears below ~ 35 at% Zr(4.6).

The compositional dependent trend has been interpreted as due to changes in the bare density of states at the Fermi energy $N^b(0)$(4.7). This is supported by ultraviolet photoelectron spectroscopy (UPS) measurements and band structure calculations(4.8). The binding energy of the d band is related qualitativily to the late transition metal; while the Zr 4d contribution to $N^b(0)$ is found to be roughly constant, the late transition metal contribution increases on going from Cu- to Ni- to Co- to Fe-Zr.

Analysis of the results in the above work was done using the McMillan equation described in Chapter 1. However results from Fe-Zr (and perhaps Co-Zr) can not be interpreted in such a simple manner. Here T_c falls much faster with composition than in Cu-Zr or Ni-Zr, while the density of states does not$^{(4.6)}$. This is interpreted as being due to magnetic effects$^{(4.7)}$, either localized magnetic moments or spin-fluctuations.

Localized magnetic moments can be ruled out because of an upper bound imposed by temperature dependent susceptibility. By estimating an upper bound to the slope of χ with temperature and treating the system as Curie-Weiss we get a generous upper bound of the number of localized magnetic moments of the system. For $Fe_{25}Zr_{75}$, where the effect should be the largest of the systems measured, temperature dependent susceptibility measurements$^{(4.9)}$ lead to an estimate of an upper bound of less than 5 ppm localized magnetic moments, ie. fewer than the resolution of the test. This leads to the conclusion that localized magnetic moments are not responsible.

On the other hand clear evidence for spin-fluctuations in amorphous Fe-Zr has been seen on examining temperature dependent resistivity$^{(4.10)}$. The authors find that at higher concentrations of iron the low-temperature resistivity behaves differently from that of other materials. With increase of temperature the resistivity first increases before decreasing as expected. The authors show clearly that the resistivity $\Delta\rho(T) = \rho(T) - \rho(4.2)$ can be fit to the curve of $\Delta\rho(T)$ vs T due to spin-fluctuations(4.11).

Before turning to the effects of relaxation it is worth remarking that the effects in Co-Zr, as one would expect, lie between Fe-Zr and Ni- and Cu-Zr, and the extent to which spin-fluctuations are important is debatable. However at the zirconium compositions of interest in the present work all authors agree that magnetic effects are small(4.6)(4.7).

If the difference in behaviour of T_c in Fe-Zr described above is due to spin-fluctuations then one may expect in this system a different sensitivity to thermal annealing. Annealing a sample at temperatures well below the crystallization temperature induces small structural changes in the glass. The effects of small structural changes can thus be examined without the added complication of changes in composition. Many workers in the field have examined the effects of annealing, both for reversible and irreversible changes in structure. Reversible relaxation is discussed in section 4.3.

Work done to determine the effect of low temperature annealing includes systems such as Zr-based glasses(4.12)(4.13). Zirconium-rich alloys have been used and T_c, measured resistively, measured to monitor changes in the alloys. Upon long time annealing of the alloys for very low anneal temperatures, T_c was found to saturate. Differences in the tendencies to saturate are ascribed to differences in crystallization at this stage. The present work does not support this interpretation as in the present work there is no evidence of any crystallization for such short periods of annealing.

We now present a brief summary of the influence of spin-fluctuations on superconductivity. The effect of spin-fluctuations is simple: whereas the attractive electron interaction is phonon mediated and works between pairs of electrons with anti-parallel spins, spin-fluctuations arise from an electron-electron intra-band interaction. A second electron of opposite spin is attracted to a first electron via phonons. Near the first electron there is a large number of electrons with parallel spins and this hinders the second electron from following the first electron. The two electrons then have a smaller effective attraction. Thus the electron-phonon interaction is effectively decreased, depressing superconductivity. Because this interaction is most effective where electron spins can align ferromagnetically it has its greatest effect for strongly enhanced paramagnets.

The spin-fluctuation interaction for transition metals was introduced numerically(4.14) into the McMillan equation (equation 1.5). This approach proved useful for some materials, as evidenced by the fact that the electron-phonon interaction parameter now varied regularly with valence for the transition metals, which, although expected, was not possible with the simpler expression.

It was later shown(4.15) that the effect of spin-fluctuations could be included analytically in the McMillan equation by renormalizing the electron-phonon (mass-enhancement) interaction parameter λ_{ep} by a spin-fluctuation mass enhancement parameter λ_{sf} (see below). In the model λ_{ep} is renormalized to $\frac{\lambda_{ep}}{1+\lambda_{sf}}$ and μ^* is enhanced and renormalized to $\frac{\mu^*+\lambda_{sf}}{1+\lambda_{sf}}$. Substituting these new forms for λ_{ep} and μ^* into equation (1.5) results in the modified McMillan expression:

$$T_c = \frac{\Theta_D}{1.45} \exp\left(-\frac{1+\lambda_{ep}+\lambda_{sf}}{\lambda_{ep}-\lambda_{sf}-\mu^*}\right) \tag{4.4}$$

In the McMillan expression the top line in the exponential is the electron mass-enhancement factor which is now enhanced further by λ_{sf}, the spin-fluctuation mass enhancement parameter; the bottom line contains the effective coupling which is reduced by λ_{sf}. It should be noted that this simple expression has been critisized by Leavens and MacDonald(4.16) who point out that more information about the spin-fluctuations is required (e.g. a characteristic frequency). Thus equation 4.4 must be regarded as an approximation.

λ_{sf} is given by(4.17)(4.18):

$$\lambda_{sf} = \frac{9}{2}\,\bar{I}\,\ln\left(1+\frac{p_1^2}{12}\,\frac{\bar{I}}{(1-\bar{I})}\right) \tag{4.5}$$

p_1 is the momentum cutoff factor for spin-fluctuations, the upper limit to the momentum of spin-fluctuations expressed as a fraction of k_F. $\bar{I}$ is the Stoner enhancement factor for the valence (Pauli) magnetic susceptibility which results from the intra-band exchange interaction. The enhanced valence susceptibility can be written as:

$$\chi_v = \frac{\mu_B^2 \, N^b(0)}{1-\bar{I}} \tag{4.6}$$

Here $N^b(0)$ is the bare density of electron states in units of $\frac{\text{states}}{\text{erg mole}}$ at the Fermi energy E_F, and μ_B, the Bohr magneton, is in units of $\left(\frac{\text{erg}}{\text{G}}\right)^2$. $N^b(0)$ can not easily be measured directly except by electron tunneling. However the mass enhancement density of states $N^\lambda(0) = N^b(0)(1+\lambda_{ep}+\lambda_{sf})$ can be measured by specific heat or, as in the present case, by measuring the upper critical field as a function of temperature. Since amorphous superconductors are type II, as discussed in Chapter 1, to extract $N^\lambda(0)$ one must use the following equations$^{(4.19)}$ which are valid for superconductors in the 'dirty' limit:

$$N^\lambda(0) = -(9.451\text{x}10^{-10})\frac{M}{\rho d}\left(\frac{dH_{c2}}{dT}\right)_{T_c} \tag{4.7}$$

$$N^b(0) = \frac{N^\lambda(0)}{(1+\lambda_{ep}+\lambda_{sf})} \tag{4.8}$$

in units of $\frac{\text{states}}{\text{eV atom}}$, where M = molecular weight; the resistivity ρ is measured at 4.2 K in Ω-cm; d = density in g/cm^3. A value for the valence susceptibility (χ_v) can be found by measuring the total susceptibility χ and using

$$\chi = \chi_v + \chi_{core} + \chi_{VV} \tag{4.9}$$

Contributions to the total susceptibility are as follows: the valence susceptibility χ_v; χ_{core} is the diamagnetic core, or Larmor, susceptibility, which is due to the filled shells of electrons; and χ_{VV} which is the Van Vleck paramagnetic susceptibility, the correction to the core susceptibility for atoms with unfilled electron shells.

By manipulating the formulae above, it is possible to obtain values for N^b, $\bar{I}$, λ_{ep}, and λ_{sf}. Thus, knowing T_c, χ, and $\left(\frac{dH_{c2}}{dT}\right)_{T_c}$, it is possible to estimate the magnitude of the electron-phonon and spin-fluctuation parameters. These equations were used by Altounian and Strom-Olsen(4.6)(4.20) in their analysis of the composition dependence of T_c in Cu-Zr, Ni-Zr, Co-Zr, and Fe-Zr. These authors used the following values of the unknown parameters. μ^*, as is usually done for zirconium(4.21) systems was approximated by the constant 0.13. Note that the constant 0.13 is not an experimentally known quantity, but rather is consistent for all 4d superconducting systems. The momentum cutoff factor for spin-fluctuations was taken as $p_1^2 = 1/6$. Again, this is not an experimentally known quantity, but, chosen as 1/6, leads to consistent analyses for zirconium-based systems(4.22). The diamagnetic core, or Larmor, susceptibility, is typically $= -20 \times 10^{-6}$ emu/mole for Zr and $= -29 \times 10^{-6}$ emu/mole for Fe, while the most consistent results(4.20)(4.23) for the Van Vleck susceptibility indicate that the latter is typically $= 115 \times 10^{-6}$ emu/mole for Zr and negligible for Fe for low Fe concentrations.

Values for the Van Vleck term are not obvious, since this term can not be measured directly. The cited values were obtained from analysis of data of the Knight shift in amorphous Cu-Zr, measured by NMR. Since the values are difficult to obtain and can not easily be verified they are probably inaccurate. Small errors in χ_{core} and χ_{VV} are not important in the present work because we look at changes with annealing and there is no evidence to suggest that either χ_{core} or χ_{VV} changes significantly upon annealing. An error in these values would induce an offset in the results but would not upset the trends in results. If these values do change significantly upon annealing then the analysis presented here for annealed samples would have to be modified for more meaningful results.

Table 4.1 shows the values for $N^b(0)$, $\bar{I}$, λ_{ep}, and λ_{sf} for zirconium-rich Fe-Zr. Values quoted are for as quenched samples and for those annealed at 488 K for 500 minutes. The anneal time was chosen to be before the break in the curve of T_c vs t_{anneal} for $Fe_{22.5}Zr_{77.5}$ and $Fe_{25}Zr_{75}$ samples and after the break for both $Fe_{20}Zr_{80}$ #1 and #2. $Ni_{25}Zr_{75}$ is included for comparison. Values of T_c, χ, and $\left(\frac{dH_{c2}}{dT}\right)_{T_c}$ are taken from the data presented in Chapter 3. It should be noted, however, that the values obtained are not exact since a number of approximations were made to arrive at the equations. The calculations show that for each sample the values of $N^b(0)$, λ_{sf}, and perhaps λ_{ep}, presented in table 4.1,

Table 4.1

Calculated values of N^b, $\bar{I}$, λ_{ep}, and λ_{sf}

sample	$N^b\left(\frac{\text{states}}{\text{eV-atom}}\right)$	$\bar{I}$	λ_{ep}	λ_{sf}
as quenched				
$Fe_{20}Zr_{80}$ #1	1.413±0.05	0.581±0.015	0.618±0.01	0.050+-0.005
$Fe_{20}Zr_{80}$ #2	1.462	0.592	0.591	0.053
$Fe_{22.5}Zr_{77.5}$	1.291	0.699	0.661	0.100
$Fe_{25}Zr_{75}$	1.395	0.688	0.603	0.093
$Ni_{25}Zr_{75}$	1.359	0.267	0.551	0.006
annealed				
$Fe_{20}Zr_{80}$ #1	1.362	0.554	0.610	0.043
$Fe_{20}Zr_{80}$ #2	1.346	0.595	0.600	0.054
$Fe_{22.5}Zr_{77.5}$	1.210	0.628	0.613	0.066
$Fe_{25}Zr_{75}$	1.355	0.666	0.598	0.082
$Ni_{25}Zr_{75}$	1.418	0.224	0.538	0.004

decrease upon annealing. While there is a consistent decrease in the values, this decrease is only just above the error. The large error is mostly due to error in upper critical field measurements which were used in the calculations. The trends in values of λ_{ep} and λ_{sf} with iron concentration support the findings; with increased iron concentration there is an increase in λ_{sf}. Since the spin fluctuation interaction is due to the iron in the sample, with more iron we expect a larger effect, as was found. For comparison, the same analysis was performed for $Ni_{25}Zr_{75}$. As expected, although values for $N^b(0)$ and λ_{ep} are comparable to those for Fe-Zr, the spin-fluctuation parameter is almost nonexistant. Note also that the changes in both $N^b(0)$ and λ_{ep} with annealing are comparable for both systems. This strongly supports the argument for spin-fluctuations.

Annealing a sample has the effect of reducing the density of states. A decrease in $N^b(0)$ lowers both λ_{ep} and λ_{sf}; depressing λ_{ep} reduces T_c, whereas depressing λ_{sf} raises T_c. For $Cu_{25}Zr_{75}$, $Ni_{25}Zr_{75}$, and $Co_{25}Zr_{75}$, where spin-fluctuations are not in evidence, annealing only induces a decrease in λ_{ep} so T_c decreases as was shown. For Fe-Zr, where spin-fluctuations are present, annealing induces a decrease in both λ_{ep} and λ_{sf}. For short anneals the change in λ_{sf} dominates, resulting in an increase in T_c. For longer anneals the change in λ_{ep} dominates, resulting in a decrease in T_c. It should be noted that the turnover from increasing to decreasing with anneal time is concentration dependent. The fact that this turnover point occurs at much shorter anneal times for the lower concentrations of iron indicates that the turnover is caused by a saturation of λ_{sf}, so at the longer anneal times only λ_{ep} is affected and T_c decreases.

Spin-fluctuations also explain the break in the trend of increasing T_c going from $Cu_{25}Zr_{75}$ to $Ni_{25}Zr_{75}$ to $Co_{25}Zr_{75}$ to $Fe_{25}Zr_{75}$ for the as quenched alloys. The increase in T_c with decrease in valence of the 3d element is due to an increase in the electronic density of states with a subsequent increase in λ_{ep}; the decrease seen in $Fe_{25}Zr_{75}$ is due to the added enhancement of λ_{sf} and the subsequent depression of superconductivity.

4.3 Reversible Relaxation

Besides the irreversible interactions described above, experiments have been performed to provide insight into the reversible component of structural relaxation. It has been demonstrated unequivocally that there is a small reversible relaxation effect(4.24). Research has been done to understand the nature of this reversible process but so far there has been no satisfactory explanation.

The idea that the reversible relaxation is controlled by changes in chemical short range order (CSRO) has been promoted(4.25). CSRO desribes the situation where the chemical composition around the atoms of each alloying element is different from the random average. It has been suggested(4.25) that changes in CSRO could occur by small cooperative rearrangement of atoms. In the model of CSRO it is assumed that in most cases only the nearest neighbour shell contributes to changes in observed properties due to CSRO.

An alternate mechanism for the reversible process to occur is that the reversible effect could occur by diffusive jumps(4.26) which are governed by defects moving in a similar manner to vacancies in crystals. Analysis suggests that consecutive atomic jumps occur on a mean time of ~ 10 minutes and that the diffusion coefficient is consistent with the kinetics of CSRO.

A third proposal(4.27) makes use of a simplified energy function dU and assumes that the relaxation behaviour of an amorphous material can be described qualitatively in terms of energy barriers. When a sample is at a low temperature it could be expected to lie at a local minimum of dU. If energy is imparted to the system it could be expected to overcome an energy barrier, moving to a different energy level, and, if rapidly quenched, would remain at the other energy level. In this way a sample could be annealed reversibly between energy levels. A possible mechanism for this process could be the diffusion jumps mentioned above. The authors(4.27) investigate the reversible relaxation behaviour of $Ni_{24}Zr_{76}$ using the superconducting transition temperature T_c as a monitor of relaxation. The behaviour is examined in much the same way as in the present work and a reversible component to the relaxation is found.

The above discussion leads to an analysis of our results for reversible relaxation. The results obtained demonstrate that in the systems examined where there was any reversible relaxation at all it was not a very large effect. In fact it was only just seen above the noise inherent in the experiment. Other workers(4.13) have monitored reversible relaxation using the superconducting transition temperature and also noticed that it is not greatly affected, being small compared to the irreversible component.

The alloys $Ni_{33}Zr_{67}$, $Cu_{33}Zr_{67}$, and $(CuNi)_{33}Zr_{67}$ were first examined. This was done similarly to the method used by other workers(4.27) and is described in Chapter 3. We found upon annealing cyclically between two temperatures after an initial series of anneals that in both $Ni_{33}Zr_{67}$ and $Cu_{33}Zr_{67}$ there was a small reversible component of relaxation, only just above the resolution of the experiments; in $(CuNi)_{33}Zr_{67}$ none was detected. It is possible that the reversible component of $(CuNi)_{33}Zr_{67}$, if present, went undetected because of the uncertainty in the measurements. If $(CuNi)_{33}Zr_{67}$ has a reversible component of relaxation, however, it must be smaller than that of either $Cu_{33}Zr_{67}$ or $Ni_{33}Zr_{67}$. This finding is contrary to what one would expect from the CSRO model which indicates that two similar elements in a glass would lead to greater changes in CSRO with annealing than glasses with only one of the elements.

Instead of CSRO it is possible to consider the reversible relaxation in terms of diffusion of one or two elements into the other element. A comparison of diffusion rates of Cu, Ni, Co, and Fe in amorphous Zr was not possible. If we look at their diffusion rates in α-Zr(4.28) we find that at ~ 830° C they are roughly the same. If one were to conjecture how their diffusion rates would compare in amorphous Zr one would guess that again they are on the same order but that perhaps the diffusion rates increase slightly on going from Fe and Co, to Ni and Cu because Ni and Cu have closed d-shells in amorphous zirconium glasses whereas Co and Fe have open d-shells; so one would expect Ni and Cu to interact less with, and therefore have a greater mobility in, amorphous Zr. If this were the origin of reversible relaxation then one would not expect $(CuNi)_{33}Zr_{67}$ to have a greater reversible component than either $Cu_{33}Zr_{67}$ or $Ni_{33}Zr_{67}$.

The systems $Ni_{24}Zr_{76}$, $Co_{25}Zr_{75}$ and $Fe_{25}Zr_{75}$ were then examined for reversible relaxation and the results compared. It was found that although $Ni_{24}Zr_{76}$ had a large reversible component relative to that of $Ni_{33}Zr_{67}$, neither $Co_{25}Zr_{75}$ nor $Fe_{25}Zr_{75}$ displayed any signs of one. The effect seen in $Ni_{24}Zr_{76}$ was somewhat smaller than reported in reference 4.27. In light of the diffusion argument, presented above, it is not surprising that $Ni_{24}Zr_{76}$ displayed signs of reversibility while neither $Co_{25}Zr_{75}$ nor $Fe_{25}Zr_{75}$ did.

Chapter 5 - Conclusion

The effects of annealing on the superconducting transition temperature, T_c, of X-Zr (X = Fe, Co, Ni, Cu) metallic glasses at close to 75 at% Zr has been examined. It was found that while T_c in Cu-, Ni-, and Co-Zr, as is usual, decreased on annealing, in Fe-Zr T_c increased for short anneal times, the first time that such an effect has been seen. All systems showed a logarithmic dependence on anneal time and none exhibited any tendency for T_c to saturate. In the three systems where T_c decreased on annealing, the greatest effect was observed in Cu-Zr and the least in Co-Zr.

A more detailed examination was made in $Ni_{25}Zr_{75}$ and several samples of Fe-Zr between 75 and 80 at% Zr. Changes in T_c were analyzed through the McMillan equation, suitably modified to take account of spin-fluctuations via a spin-fluctuation mass enhancement parameter λ_{sf}. It was found that in both systems the electron-phonon coupling decreases but that in Fe-Zr this decrease is more than offset by a corresponding decrease in λ_{sf} which effectively enhances superconductivity. Inclusion of a spin-fluctuation term in the McMillan equation for T_c adequately described the behaviour of Fe-Zr in the compositions studied.

Besides this irreversible component of relaxation a reversible component was sought. While a small reversible change in T_c was found for both Ni-Zr and Cu-Zr, none was found in the similar ternary glass

(CuNi)-Zr. Also no reversible change was found in either Co-Zr or Fe-Zr. The results, although not conclusive, indicate that the reversible component of relaxation is not due to chemical short range order (CSRO), but rather due to differences in diffusion rates of the 3d element in amorphous zirconium.

References

1.1 J. Kramer, Ann.Phys. 19, 37 (1934); J. Kramer, Z.Phys. 106, 675 (1937)

1.2 W. Klement Jr., R.H. Willens, P. Duwez, Nature 187, 869 (1960)

1.3 T. Egami, Mater.Res.Bull. 13, 557 (1978)

1.4 A.C. Anderson, C.C. Koch, J.O.Scarbrough, Phys.Rev.B 26, 1156 (1982)

1.5 T. Egami, Amorphous Metallic Alloys, ed. F.E. Luborsky, Ch.7, Butterworths, London, 1983.

1.6 B.S. Berry, W.C. Pritchet, Phys.Rev.Lett. 34, 1022 (1975); V.Chambron, A. Chamberod, Solid State Commun. 35, 61 (1980)

1.7 D.M. Kroeger, C.C. Koch, J.O. Scarbrough, C.G. McKamey, Phys.Rev.B 29, 1199 (1984)

1.8 L.P. Gor'kov, Zh.Eksperim.i.Theor.Fiz. 36, 1918 (1959). Eng. transl.: Soviet Phys. - JETP 9, 1364 (1959)

1.9 E. Domb, W.L. Johnson, J.Low Temp.Phys. 33, 29 (1978); R. Koepke, G. Bergmann, Solid State Commun. 19, 435 (1976)

1.10 N.W. Ashcroft, N.D. Mermin, Solid State Physics, Ch.17, Saunders College, Philadelphia, 1976

1.11 J. Bardeen, L.N. Cooper, J.R. Schrieffer, Phys.Rev. 106, 162 (1957); 108, 1175 (1957)

1.12 G.M. Eliashberg, Zh.Eksperim i. Teor. Fiz. 38, 966 (1960); 39, 1437 (1960). Eng. transl.: Soviet Phys. - JETP 11, 696 (1960); 12, 1000 (1961);
A.B. Migdal, Zh.Eksperim. i. Teor. Fiz. 34, 1438 (1958) Eng. transl.: Soviet Phys. - JETP 7, 996 (1958)

1.13 V.L.McMillan, Phys.Rev. 167, 331 (1968)

2.1 Z. Altounian, private communication

2.2 H.P. Klug, L.E. Alexander, X-Ray Diffraction Procedures, Ch.5, Wiley Interscience, New York, 1974

2.3 R. Richter, M.Sc. Thesis, McGill University, Montreal, 1984

2.4 G.K. White, Experimental Techniques in Low-Temperature Physics, pp.104-105, Oxford University Press, London, 1959

2.5 C.J. O'Connor, Progress in Inorganic Chemistry, ed. S.J. Lippard, 29, pp.216-218, Wiley Interscience, New York, 1982

2.6 A. Cambron, M.Sc. Thesis, McGill University, Montreal, 1986

3.1 Z. Altounian, J.O. Strom-Olsen, Phys.Rev.B 27, 4149 (1983)

3.2 S.J. Poon, Phys.Rev.B 27, 5519 (1983)

3.3 Z. Altounian, C.A. Volkert, J.O. Strom-Olsen, J.Appl.Phys. 57, 1777 (1985)

4.1 see ref. 3.3

4.2 K. Samwer, H.v. Löhneysen, Phys.Rev.B 26, 107 (1982);
G. von Minnigerode, K. Samwer, Physica B 108, 1217 (1981)

4.3 Z. Altounian, Tu Guo-hua, J.O. Strom-Olsen, Solid State Commun. 40, 221 (1981)

4.4 D.G. Onn, L.Q. Wang, Y. Obi, K. Fukamichi, J.Non-Crystal.Sol. 61&62, 1149 (1984);
D.G. Onn, L.Q. Wang, K. Fukamichi, Solid State Commun. 47, 479 (1983)

4.5 M.G. Karkut, R.R. Hake, Phys.Rev.B 28, 1396 (1983)

4.6 see ref. 3.1

4.7 M. Tenhover, W.L. Johnson, Physica B 108, 1221 (1981)

4.8 V.L. Moruzzi, P. Oelhafen, A.R. Williams, R. Lapka, H.-J. Güntherodt, J. Kübler, Phys.Rev.B 27, 2049 (1983);
P. Oelhafen, Glassy Metals II, ed. H. Bech, H.-J. Güntherodt, Ch.9, Springer-Verlag, Berlin, 1983

4.9 D.V. Baxter, private communication

4.10 J.O. Strom-Olsen, Z. Altounian, R.W. Cochrane, A.B. Kaiser, Phys.Rev.B 31, 6116 (1985)

4.11 A.B. Kaiser, S. Doniach, Int.J.Magn. 1, 11 (1970)

4.12 see ref. 3.2

4.13 S.J. Poon, Amorphous Metallic Alloys, ed. F.E. Luborsky, Ch.22, Butterworths, London, 1983

4.14 N.F. Berk, J.R. Schrieffer, Phys.Rev.Lett. 17, 433 (1966);
M.A. Jensen, K. Andres, Phys.Rev. 165, 545 (1968)

4.15 J.M. Daams, B. Mitrovic, J.P. Carbotte, Phys.Rev.Lett. 46, 65 (1981)

4.16 C.R. Leavens, A.H. MacDonald, Phys.Rev.B 27, 2812 (1983);
see also D.M. Burnell, John Zasadzinski, R.J. Noer, E.L. Wolf, G.B. Arnold, Solid State Commun. 41, 637 (1982)

4.17 T.P. Orlando, M.R. Beasley, Phys.Rev.Lett. 46, 1598 (1981);
J.R. Schrieffer, J.Appl.Phys. 39, 642 (1968)

4.18 S. Doniach, S. Engelsberg, Phys.Rev.Lett. 17, 750 (1966)

4.19 Equations of the Ginzburg-Landau-Abrikosov-Gor'kov theory, as presented by T.P. Orlando, E.J. McNiff Jr., S. Foner, M.R. Beasley, Phys.Rev.B 19, 4545 (1979)

4.20 E. Batalla, Z. Altounian, J.O. Strom-Olsen, Phys.Rev.B 31, 577 (1985)

4.21 H. Rietschel, H. Winter, Phys.Rev.Lett. 43, 1256 (1979);
H. Rietschel, H. Winter, W. Reichardt, Phys.Rev.B 22, 4284 (1980);
ref. 4.7

4.22 see ref. 2.1

4.23 H.-J. Eifert, B. Elschner, K.H.J. Buschow, Phys.Rev.B 25, 7441 (1982)

4.24 see ref. 1.3

4.25 see ref. 1.5

4.26 A.L. Greer, J.Non-Crystal.Sol. 61&62 737 (1984)

4.27 see ref. 1.4

4.28 G.M.Hood, R.J. Schultz, Acta Metal. 22, 459 (1974)